Helsinki University of Technology Laboratory of Space Technology
Espoo, May 2005 REPORT 55

SURFACE WATER QUALITY ESTIMATION USING REMOTE SENSING IN THE GULF OF FINLAND AND THE FINNISH ARCHIPELAGO SEA

Yuanzhi Zhang

Thesis for the degree of Doctor of Science in Technology

Helsinki University of Technology Laboratory of Space Technology
Espoo, May 2005 REPORT 55

SURFACE WATER QUALITY ESTIMATION USING REMOTE SENSING IN THE GULF OF FINLAND AND THE FINNISH ARCHIPELAGO SEA

Yuanzhi Zhang

Dissertation for the degree of Doctor of Science in Technology to be presented with due permission of the Department of Electrical and Communications Engineering, for public examination and debate in Auditorium S1 at Helsinki University of Technology (Espoo, Finland) on the 17th of June, 2005, at 12 o'clock noon.

Helsinki University of Technology
Department of Electrical and Communications Engineering
Laboratory of Space Technology

Teknillinen korkeakoulu
Sähkö- ja tietoliikennetekniikan osasto
Avaruustekniikan laboratorio

Helsinki University of Technology

Mailing address:
Laboratory of Space Technology
P.O. Box 3000
FIN-02015 HUT
Finland

Street address:
Otakaari 5A
FIN-02150 Espoo

Tel. +358 9 451 2378
Fax +358 9 451 2898

Email: yuanzhi.zhang@tkk.fi
http://www.space.hut.fi

ISBN 951-22-7718-2 (printed)
ISBN 951-22-7719-0 (electrical)
ISSN 0786-8154

Picaset Oy
Helsinki 2005

Table of Contents

PREFACE

The work presented in this thesis was carried out in the Laboratory of Space Technology, Helsinki University of Technology (HUT) in Espoo, Finland, from 1998 to 2003. All the papers presented in this thesis are closely related to the EU project "Satellite Remote Sensing for Lake Monitoring (SALMON)" (EU Contract ENV4-CT96-0311) and the Finnish national TEKES-funded project "Operative Monitoring System for Water Areas".

I would like to thank Professor Martti Hallikainen who provided me with the opportunity to carry out this work and supervised the whole work. I am grateful to Professor Jouni Pulliainen who instructed the research and commented all manuscripts. I would also like to thank Sampsa Koponen who helped me in data extraction and data analysis, as well as some scientific suggestions and discussions. Special thanks are due to the whole personnel of the Laboratory of Space Technology for a friendly working environment.

This work was also financed in part by Maj and Tor Nessling Foundation. Its support is highly appreciated.

Finally, I thank my friends, parents and sisters for their encouragement. My deepest gratitude, however, belongs to my wife, Qiaoling Chen, for her love and support; to my lovely son and daughter, Xiaoran Zhang and Xiaoshi Zhang, for their bringing enjoyment during the difficult time.

Yuanzhi Zhang
Espoo, Finland, Jan. 14, 2005

ABSTRACT

This thesis deals with surface water quality estimation using remote sensing in the Gulf of Finland and the Archipelago Sea. Satellite remote sensing of water and empirical algorithms for surface water quality variables in coastal waters in the Gulf of Finland and the Archipelago Sea are explained and results from the studies in the area are presented.

Concurrent *in situ* surface water measurements, AISA data, Landsat TM data, ERS-2 SAR data, AVHRR and MODIS data were obtained for selected locations in the Gulf of Finland and the Archipelago Sea in August 1997 and from April to May 2000, respectively. The AISA, TM, SAR, AVHRR and MODIS data from locations of water samples were extracted and digital data were examined. Significant correlations were observed between digital data and surface water quality variables. Semi-empirical, simple and multivariate regression analyses, and neural network algorithms were developed and applied in the study area. Application of neural networks appears to yield a superior performance in modelling radiative transfer functions describing the relation between satellite observations and surface water characteristics. The results show that the estimated accuracy for major characteristics of surface waters using the neural network method is much better than retrieval by using regression analysis. Since radar observations of water are strongly affected by surface geometry but not by water quality, radar data should be useful to eliminate the effects of surface roughness from the results when combined with optical observations. However, our results suggest that microwave data improve estimation of water quality very little or not at all. The technique, however, should be examined with new data sets obtained under various weather and water quality conditions in order to estimate its feasibility for estimating surface water quality parameters in the Finnish coastal waters.

LIST OF ACRONYMS

AISA	Airborne Imaging Spectrometer for Applications
ASAR	Advanced Synthetic Aperture Radar
AVHRR	Advanced Very High Resolution Radiometer
Chl-a	Chlorophyll-a
CZCS	Coastal Zone Color Scanner
DN	Digital Number
EM	Electromagnetic
ENVISAT	ENVISAT Satellite-1
ERS-2	European Remote Sensing-2
ERTS-1	Earth Resurces Technology Satellite-1
FNU	Formazine Nephelometric Units
FOV	Field Of View
GES DAAC	Goddard Earth Sciences Distributed Active Archive Centre
HUT	Helsinki University of Technology
IOP	Inherent Optical Properties
IR	Infrared
ISO	International Organization for Standardization
Landsat TM	Landsat Thematic Mapper
Landsat MSS	Landsat Multi-Spectral Scanner
MERIS	Medium Resolution Imaging Spectrometer Instrument
MODIS	Moderate Resolution Imaging Spectroradiometer
MRA	Multiple Regression Analysis
NIR	Near Infrared
NNE	Neural Network Estimation
NOAA	National Oceanic and Atmospheric Administration
RMSE	Root Mean Square Error
SALMON	**SA**tellite Remote Sensing for **L**ake **MON**itoring
SAR	Synthetic Aperture Radar

SDD	Secchi Disk Depth
SeaWiFS	Sea-viewing Wide Field-of-view Sensor
SRA	Simple Regression Analysis
SSC	Suspended Sediment Concentration
SSE	Sea Surface Effects
SST	Sea Surface Temperature
SWT	Surface Water Temperature
SYKE	Finnish Environment Institute
TIR	Thermal Infrared
TSS	Total Suspended Sediment
Turb	Turbidity
VNIR	Visible and Near Infrared
WQV	Water Quality Variables

LIST OF APPENDED PAPERS

This thesis is based on the work contained in the following papers, hereafter referred to papers as [P1] to [P6]:

[P1] **Zhang, Y.,** Pulliainen, J., Koponen, S., and Hallikainen, M. Empirical algorithms for Secchi disk depth using optical and microwave remote sensing data from the Gulf of Finland and the Archipelago Sea. *Boreal Environment Research,* vol. 8, no. 3, pp. 251-261, 2003.

[P2] **Zhang, Y.,** Koponen, S., Pulliainen, J., and Hallikainen, M. Application of empirical neural networks to chlorophyll-a estimation in coastal waters using optosensors. *IEEE Sensors Journal,* vol. 3, no. 4, pp. 376-382, 2003.

[P3] **Zhang, Y.,** Pulliainen, J., Koponen, S., and Hallikainen, M. Water quality retrievals from combined Landsat TM and ERS-2 SAR data in the Gulf of Finland. *IEEE Transactions on Geoscience and Remote Sensing,* vol. 41, no. 3, pp. 622-629, 2003.

[P4] **Zhang, Y.,** Pulliainen, J., Koponen, S., and Hallikainen, M. Application of an empirical neural network to surface water quality estimation in the Gulf of Finland using combined optical data and microwave data. *Remote Sensing of Environment*, vol. 81, no. 2-3, pp. 327-336, 2002.

[P5] **Zhang, Y.,** Pulliainen, J., Koponen, S., and Hallikainen, M. Water quality studies of combined optical, thermal infrared and microwave remote sensing. *Microwave and Optical Technology Letters*, vol. 34, no. 4, pp. 281-285, 2002.

[P6] **Zhang, Y.,** J. Pulliainen, S. Koponen, and M. Hallikainen, M. Detection of Sea Surface Temperature (SST) using infrared band data of Advanced Very High Resolution Radiometer (AVHRR) in the Gulf of Finland. *International*

Journal of Infrared and Millimeter Waves, vol. 23, no. 10, pp. 1407-1412, 2002.

The first author was responsible for carrying out the presented research in these six publications. The other co-authors acted as scientific advisors, gave suggestions and processed or produced data. In [P1], Yuanzhi Zhang developed and performed a semi-empirical algorithm for determining SDD in the study area and drafted the manuscript. Jouni Pulliainen modified the manuscript. Sampsa Koponen and Martti Hallikainen gave helpful suggestions to improve the manuscript. In [P2], Yuanzhi Zhang drafted the manuscript, extracted image data and performed the algorithms. Sampsa Koponen modified part of the manuscript and processed a part of the data. Jouni Pulliainen and Martti Hallikainen gave critical comments to improve the manuscript. In [P3]-[P6], Yuanzhi Zhang drafted the four manuscripts, extracted image data and performed the algorithms. Jouni Pulliainen modified the four manuscripts. Sampsa Koponen processed a part of the data and gave useful suggestions on the four manuscripts. Martti Hallikainen gave critical comments and helpful suggestions to improve all these manuscripts.

1. INTRODUCTION

This doctoral thesis describes surface water quality estimation using remote sensing in the Gulf of Finland and the Finnish Archipelago Sea. The thesis has an introductory chapter that provides the general background to satellite remote sensing of water, and a second chapter that deals with remote sensing of water including remote sensing theory for two cases of active and passive sensing, as well as comments on retrieval of water quality variables. The third chapter focuses on data sources, highlighting *in situ* data and remotely sensed data in the study area. The fourth chapter outlines methodology, especially in employing semi-empirical, multivariate regression and neural network algorithms in the study. The fifth chapter presents results and discussion for the study area using AISA, Landsat TM, ERS-2 SAR, AVHRR and MODIS data in 1997 and 2000, respectively. The sixth chapter concludes this thesis. In addition, the seventh chapter introduces future research and the eighth chapter summarizes the six papers appended in the thesis.

1.1 Satellite remote sensing of water

The use of satellite remote sensing for water quality mapping started in the 1970's by for example Strong (1974) and Klemas et al. (1974) using ERTS-1 (Earth Resources Technology Satellite, later renamed Landsat-1) data. ERTS-1, launched in August 1972, introduced remote sensing as a potential tool of environmental monitoring. A broadband Multi-Spectral Scanner (MSS) was onboard ERTS-1, by which the radiation upwelling from the sensed target was recorded within the field-of-view (FOV) of the downward-looking MSS sensor. This remotely sensed target is an environmental ecosystem including atmospheric, terrestrial, and/or aquatic regimes, for example. MSS recorded an integrated spectral signature reflected from the solar and sky radiation impinging upon the earth surface. The signal recorded at the satellite was optical information, and thus such optical data should be interpreted as optical properties of environmental targets.

Up to date, the digital evaluation of optical satellite information at visible and near infrared (NIR) wavelengths has been used to estimate water quality characteristics of surface waters, for example, Alföldi and Munday (1978), Moore (1980), Munday and

Zubkoff (1981), Gordon and Morel (1983), Lillesand *et al.* (1983), Curran and Novo, (1988), and Lindell *et al.* (1985, 1999). Such investigations also suggest that optical data such as Landsat TM and AVHRR can provide an alternative means for obtaining relatively low-cost, simultaneous information on surface water quality conditions from numerous lakes, coastal and oceanic areas, for example, Lathrop and Lillesand (1986, 1991), Dwivedi and Narain (1987), Tassan (1987), Doerffer *et al.* (1989), Braga *et al.* (1993), Dekker and Peters (1993), Lavery *et al.* (1993) and Woodruff *et al.* (1999). Although optical satellite data can present a synoptic monitoring of surface water quality, its quantitative use is still a difficult task.

Since oceanic (Case I) waters are optically simple (e.g., Morel and Prieur 1977, Gordon and Morel 1983), satellite quantification of light attenuation had focused on oceanic regions (e.g., Smith and Baker 1978, Morel 1988, Spinrad 1989, Platt *et al.* 1991), e.g. using Coastal Zone Color Scanner (CZCS) data in the past. Light attenuation in oceanic waters (e.g., Morel and Prieur 1977, Gordon and Morel 1983) is primarily related to phytoplankton pigments and their derivative products (not including water) (e.g., Smith and Baker 1978). In coastal (Case II) waters, however, light attenuation is greater due to optical complexity in the form of inorganic particulates, and due to a greater variety and higher concentration of dissolved and particulate organic matter which result from significant quantities of terrigenous materials (e.g., Woodruff *et al.* 1999). In addition, remote sensing of Case II waters is more complicated than remote sensing of Case I waters due to atmospheric correction problems not only optical complexity of Case II waters. The number of surface water quality parameters that can be derived from optical satellite data is limited. As a result, some parameters for a given site or, alternatively, some inherent optical properties (IOP) must be known (e.g., Lahet *et al.* 2000). Moreover, cloud cover in optical satellite data acquisition seriously affects the usefulness of these data for monitoring surface water quality (e.g., Lavery *et al.* 1993). In contrast, the availability of radar remote sensing is almost independent of weather conditions.

In principle, radar remote sensing is very different from optical remote sensing, since radar signals are not hindered by clouds. Furthermore, a microwave radar signal does not significantly penetrate into the water. Instead it reflects from the water surface. Synthetic aperture radar (SAR) is well known to observe water surface conditions. Since all features visible in SAR imagery of the water are necessarily surface phenomena, all structures in SAR images are mainly related to changes in the

surface roughness (e.g., Alpers *et al.* 1981, Shuchman *et al.* 1981, Vesecky *et al.* 1982, Beal *et al.* 1983, Hasselmann *et al.* 1985, Monaldo *et al.* 1986, Bruning *et al.* 1988, Nisson *et al.* 1995, Vogelzang *et al.* 1994 and 1997). Therefore, the radar backscattering signatures can only carry information regarding the characteristics of the water surface: (a) the geometry of water surface (waves and ripples); (b) material on water surface; and (c) permittivity (dielectric constant) of water (top layer) (e.g., Lindell *et al.* 1999). Nevertheless, water surface material can be related to such materials as chlorophyll-a or oil pollution and other wastes on the surface.

Optically, the Gulf of Finland and Finnish Archipelago are dominated by scattering from suspended sediments, whereas the coastal waters of the Gulf are dominated by absorption from yellow substance, phytoplankton and suspended matter. This is because the Gulf of Finland is highly affected by the input from the rivers which discharge a high concentration of mineral suspended solids and nutrients. The optical characteristics of the water have been studied by using space-borne and aircraft borne remotely sensed data in the Gulf of Finland and the Finnish Archipelago Sea (e.g., Eloheimo *et al.* 1998, Hallikainen 1999a, Pulliainen *et al.* 2001, Koponen *et al* 2001 and 2002, Erkkila and Kalliola 2004). However, due to the limited number of spectral bands available from Landsat satellite sensors, retrieval algorithms still need to be refined. Fortunately, SeaWiFS, MERIS and MODIS are able to measure surface water leaving radiance in six or more wavelengths at the visible wavelengths (McClain *et al.* 1998, O'Reilly *et al.* 1998, Ruddick *et al.* 2000, Hu *et al.* 2000) which will be taken into account in our future study. In addition, the ENVISAT satellite enables the simultaneous acquisition of SAR and optical data (ASAR and MERIS) to be further applied in the study area. So far, remotely sensed data have widely been used to estimate major water quality variables such as chlorophyll-a, turbidity, suspended sediment concentration, Secchi disk depth, surface water temperature, wave height, and sea surface roughness etc. However, literature also suggests that radiometric studies show a little usefulness in determining the taxonomic composition of the phytoplankton communities in coastal waters (e.g., Cairns *et al.* 1997).

The coastal waters of the Baltic Sea are variable in their optical properties. Despite rather low values of attenuation depth in the region, water quality can be estimated using remote sensing data (Herlevi 2002). Water quality is the general perception of a simple property that tells whether water is polluted or not. However, water quality

parameters derived from remotely sensed data in this study included chlorophyll-a, suspended sediment, turbidity, Secchi disk depth, and surface water temperature.

1.2 Earlier work in the Baltic Sea

The Baltic Sea has been studied for many years by, for example, the University of Helsinki, Tartu University, Uppsala University, Stockholm University, and other universities. They provided optical properties and concentrations of optical active substances in the Baltic (e.g., Kutser 1997, Kowalczuk 1999, Herlevi 2002, Darecki and Stramski 2004). It has been reported that the common blue-to-green ratios of ocean reflectance do not provide the best algorithm for chlorophyll-a retrieval in the Baltic (Darecki et al. 2003). A comprehensive analysis of the performance of standard algorithms should be beneficial for the current use of remote sensing and future efforts on algorithm development. However, this study also applied multivariate regression and neural network algorithms to estimate water quality parameters employing optical, thermal IR and microwave data in the area.

1.3 The objective of this study

This study is part of the EU project entitled “Satellite Remote Sensing for Lake Monitoring (SALMON)” and the Finnish project entitled “Operative Monitoring System for Water Areas”. The purpose of this study is to evaluate the capabilities and potential of present and future space-borne sensors for monitoring water quality of European lakes, especially in Finnish lakes and coastal areas in the Gulf and Archipelago of Finland (Hallikainen 1999b). In the study, both optical satellite data (e.g., Landsat TM, AVHRR and MODIS) and microwave data (e.g., ERS-2 SAR) were used to estimate surface water variables by case studies. In addition, the study investigated the possibility of combined use of optical and microwave remote sensing data, but also developed and employed empirical algorithms of estimating surface water quality variables in the area.

1.4 Research methods

During research of water quality monitoring, optical properties of waters in coastal areas and lakes in the southern Finland have been studied using airborne and satellite

sensors. This used remote sensing technology operated jointly by the Finnish Environment Institute (SYKE) and the Laboratory of Space Technology of Helsinki University of Technology (HUT) from 1996 to 1999. The HUT work share particularly included (Hallikainen 1999b):

(1) investigation of the applicability of microwave radiometer and SAR data for water quality monitoring;
(2) surface water quality parameters retrieved from microwave data and combined optical/microwave data;
(3) airborne campaigns conducted using the HUT research aircraft.

Concurrent *in situ* measurements of surface water quality were conducted by SYKE, while the processing of remotely sensed data were finished at HUT. The extraction of optical and SAR data, corresponding to *in situ* observations of surface water quality variables, was performed by using ER Mapper 5.5. Empirical algorithms were developed and performed using Matlab 6.1 at the HUT Laboratory of Space Technology. Semi-empirical, simple and multivariate regression, and neural network algorithms were applied to estimate surface water quality variables in the Gulf and Archipelago of Finland. In the developed multivariate and neural network empirical algorithms, visible/NIR, thermal IR and microwave data were used and compared. The results show that the additional use of microwave data (e.g., ERS-2 SAR data) improved the estimated accuracy of optical retrievals in a very limited way. However, the method still needs to be refined using new optical and microwave data such as MERIS and ASAR data in the future under study.

2. REMOTE SENSING OF WATER

2.1 Remote sensing theory

In remote sensing, physical phenomena are observed through properties and changes in electromagnetic (EM) radiation. This means that EM waves are carriers of information, and it is necessary to understand their interaction with matter. On the other hand, these EM waves have the following measurable properties: frequency or wavelength, polarisation and phase. These different interactions of waves with a surface or volume can be defined as: emission, absorption, reflection (scattering), refraction and transmission.

A fundamental fact is that all natural bodies emit incoherent radiant EM energy. Moreover, the energy radiated by the Sun is reflected, absorbed and scattered from atmosphere as well as from all natural bodies. A simplified theoretical schema involving these radiation mechanisms can be set up. This basic measurement configuration is shown in Figure 2.1 (Bukata *et al.* 1995).

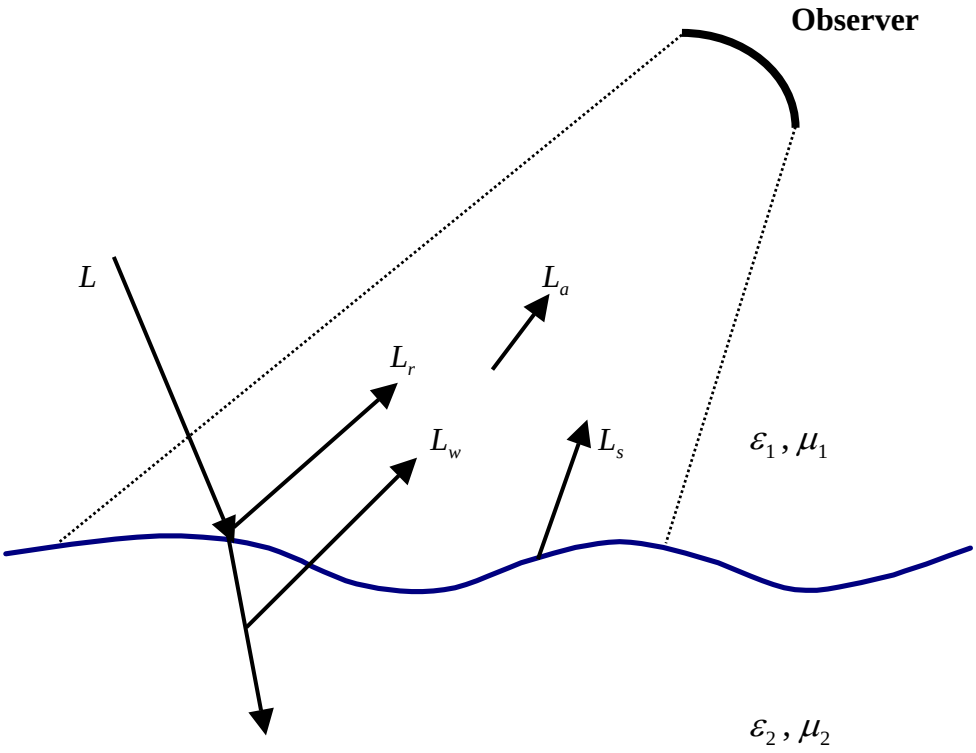

Figure 2.1: A basic remote sensing configuration.

The field of view (FOV) of the observer is shown as dashed lines. The radiance signal ($Wm^{-2}sr^{-1}Hz^{-1}$) received by the observer from a water body has components from the surface (L_s), the atmosphere (L_a), a reflected component (L_r) and a refracted and scattered component inside the water (L_w). The emitted energy (L_s) comes from the surface of the water body itself. Depending on the measured wavelength, some components are dominant. In the case of active mono-static remote sensing, the geometry changes so that L comes from the direction of the observer, and the received signal is mainly constituted of a reflected wave (L_r), possibly a refracted wave (L_w), while L_s and L_a are not so significant. Therefore, the signal (L_u) received by the observer near the water surface can be expressed as

$$L_u = L_r + L_w + L_s + L_a \quad \text{(passive case)} \tag{2.1.a}$$

$$L_u \approx L_r + L_w \quad \text{(active case)} \tag{2.1.b}$$

where L_r gives the information reflected from the water surface such as the undulation characteristics and oil slick pollution, and L_w gives information scattered from inside the water column.

In the case of passive remote sensing, if the incoming radiation from the zenith point (L_z) (i.e., directly downwards) is reflected from the nadir point (i.e., directly upwards), then the reflected part L_r can be determined as (Arst *et al.* 1997)

$$L_r \approx 0.02 L_z \tag{2.2}$$

The reflection coefficient (2% of L_z) is not dependent on the wavelength at the optical wavelengths because refraction indices of the air and water are constants. However, L_r is only valid in the case of calm water surface or low solar altitude (Arst and Kutser 1994, Arst *et al.* 1997). In other cases, the received signal may increase due to the sun glitter from the nadir. Therefore, this corresponding error increases with the rise of the wind speed and high solar altitude.

Suppose E_d is the spectral downwelling irradiance and L_u is the upwelling radiance, and further suppose L_r and L_w are known. Therefore, the spectral reflectance of water components can be determined by (Kutser 1997)

$$R(\lambda) = \frac{\pi L_u(\lambda)}{E_d(\lambda)} = \frac{\pi L_r(\lambda)}{E_d(\lambda)} + \frac{\pi L_w(\lambda)}{E_d(\lambda)} = R_r + R_w \qquad (2.3)$$

where R_r and R_w are the reflectance from the water surface and from water column respectively.

On the other hand, the emitted spectral brightness B_f ($Wm^{-2}sr^{-1}Hz^{-1}$) from the surface (L_s) is defined as, according to Planck's blackbody radiation law (e.g. Ulaby 1981, Nyfors and Vainikainen 1989)

$$B_f = \frac{2hf^3}{c^2}\left(\frac{1}{e^{\frac{hf}{kT}} - 1}\right) \qquad (2.4)$$

where *k* is Planck's constant, *T* is the physical temperature of the water body and *f* is frequency. In practice, the brightness temperature T_b is used instead of spectral brightness. The brightness temperature T_b represents the intensity of the observed radiation and is defined as

$$T_b(\varphi,\theta) = eT(\varphi,\theta) \qquad (2.5)$$

where *e* is the emissivity of the medium and *T* is physical temperature. The emissivity is a value between 0 and 1 and, theoretically, can be 0 for a perfect conductor and 1 for a perfect black body. For all natural objects it is less than 1, therefore the brightness temperature is always lower than the physical temperature. Moreover, the emissivity is a function of frequency and material properties, of which the dielectric coefficient of the medium is the most significant when using microwaves. In addition, the brightness temperature is dependent on the angle of observation as shown in Figure 2.2 (a) and 2.2 (b).

The component defined as L_r in Figure 2.1 represents reflected energy from an outside source. In addition to reflection, part of the downwelling energy will be absorbed, refracted and eventually scattered upwards (L_w). The reflection phenomena can be approximated using two parts: specular reflection and scattering from a rough surface. These two components are represented in Figure 2.3 (a) and 2.3 (b). In the

specular case of Figure 2.3 (a), the reflection coefficient r_0 can be determined using the elementary Fresnels' formulas. These formulas can be briefly expressed as

$$r_0 = r_0(p, \varepsilon_r, \theta) \tag{2.6}$$

This means that they are functions of polarisation *p*, dieletric permittivity ε_r, and incident angle θ.

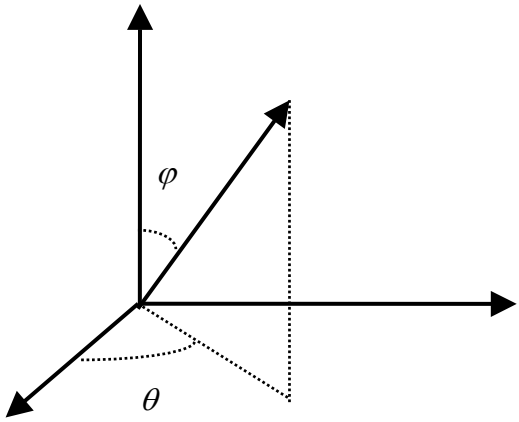

Figure 2.2 (a): Coordinate system for Figure 2.2 (b).

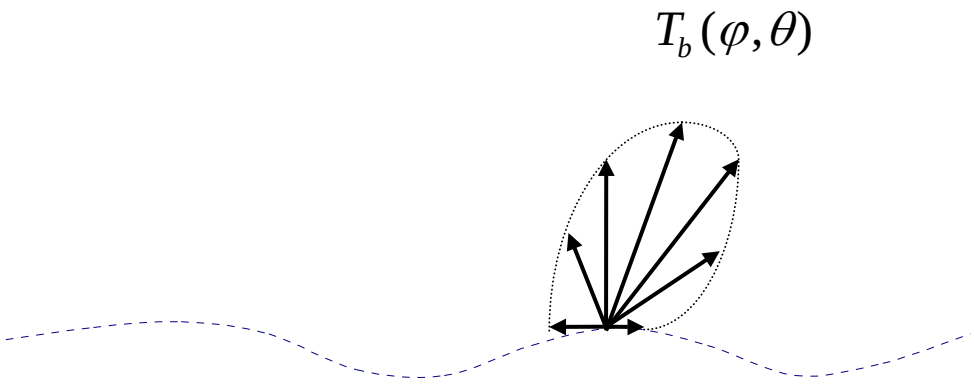

Figure 2.2 (b): The angular brightness temperature distribution of a semi-infinite isothermal medium.

However, scattering from a rough surface is more complex and highly dependent on observed wavelength. Theoretical, semi-empirical and empirical models can be found in the literature (e.g., Ulaby 1981, Nyfors and Vainikainen 1989, Chen 1992,

and Broschat 1993). A simple semi-empirical model will be presented here to show an overview of the problem. The scattered component S including coherent and incoherent contributions can be defined as

$$S = r_0 P_i G \tag{2.7a}$$

$$L(r,\hat{s}) = \frac{dP}{\cos\theta * da * d\omega * df} \tag{2.7b}$$

where $L(r,\hat{s})$ is radiance at a point r in a random medium measured in $Wm^{-2}sr^{-1}Hz^{-1}$ (sr = steradiance = unit solid angle) and dP is the power measured in watts flowing within a solid angle $d\omega$ through an elementary area da oriented in a direction of unit vector $\hat{s}_0$ in a frequency interval $(f, f+df)$ (Ishimaru, 1978). This equation gives the relation between radiance (L) and power (P) used in the study.

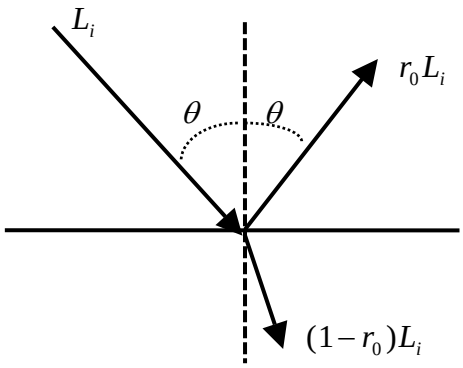

Figure 2.3 (a): Specular reflection and transmission.

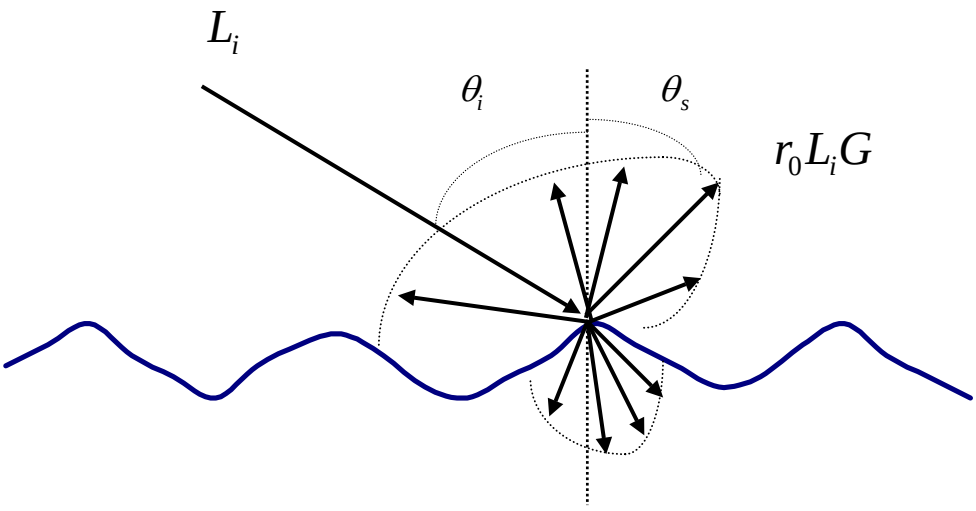

Figure 2.3 (b): Scattering and transmission from a rough surface.

In Figure 2.3 (b) L_i is the incoming wave, r_0 is the specular reflection factor and G is unknown function. The latter can be expanded in an exponential function with F dependent on wavelength, incoming angle, rms. height of surface roughness, and polarisation. That is, G could be expressed as (Broschat 1993)

$$G = \exp\left[-F(\lambda, \sigma_h, \theta, p)\right] \tag{2.8}$$

where λ is the wavelength, σ_h is the rms. deviation of surface roughness, θ is the incident angle and p is a polarisation. Because the roughness is determined by the wavelength used to make measurements, a more precise approach would be needed for different remote sensing instruments. So far, the components marked L_a in Figure 2.1 have been ignored. This means that the emission and scattering by the atmosphere will be skipped here. In fact, significant contribution of signal at visible wavelengths received by a satellite sensor originates from the atmosphere. This effect should be removed before data analysis. It is generally assumed in the atmospheric models that water-leaving radiance is zero in the near infrared part of spectrum (e.g., Chavez 1988). Since the data analysis is made for a single image with a quite small angular range and the infrared band is close to zero, the atmospheric correction has no effect on correlation analysis in this study. That is, the atmospheric correction for satellite optical sensors data could be ignored if only one scene of these data is used in the study. However, when multi-temporal data were used for the analysis, it is necessary to correct atmospherically.

2.2 Retrieval of water quality variables

Colour index, as a quantitative measure of ocean water colour, can be defined as the ratio of nadir radiance in the water at the blue wavelength to that at the green wavelength (Jerlov 1976). Therefore, on the basis of this definition, the chlorophyll concentration in oceanic waters can be estimated with reasonable accuracy from remotely sensed data. That is, from ratios of spectral radiance received by satellite or aircraft sensors, chlorophyll retrieval algorithms can be developed (e.g., Gordon and

Clark 1980, Morel 1980, Gordon *et al.* 1983, Tassan 1994). The algorithm is expressed as

$$C_{Chl} = x_1 \left[\frac{L_u(\lambda_1)}{L_u(\lambda_2)} \right]^{x_2} \tag{2.9}$$

where C_{Chl} means chlorophyll-a concentration, $L_u(\lambda_1)$ and $L_u(\lambda_2)$ are the upwelling radiances at wavelengths λ_1 and λ_1 respectively, x_1 and x_2 are empirical constants.

For surface water quality variables retrieved from remotely sensed data, the retrieval algorithm in general can be written as

$$C_i = aX + b \tag{2.10}$$

where C_i is a measurement of surface water quality parameters such as chlorophyll-a concentration, suspended matter, turbidity, Secchi disk depth, sea surface temperature etc., *a* and *b* are constants from correlation analyses, and *X* denotes a channel ratio $L_u(\lambda_1) \big/ L_u(\lambda_2)$. The success of such algorithms is highly correlated to the optical simplicity of open oceanic and some near-coastal waters (Kutser 1997). However, those natural waters strongly affected by the land mass have higher orders of optical complexity. This is a consequence of an increase of optically active aquatic components present in the waters and various concentration ranges of these water components. This means that these algorithms for simplistic oceanic chlorophyll retrievals cannot be directly applied to those optical properties in coastal, estuarine, lake, and river waters (e.g., Bukata *et al.* 1991, Kutser 1997). In this study, band ratios were only employed to examine variables in simple regression analysis.

On the other hand, due to the limited number of spectral bands available in satellite sensors, these retrieval algorithms still need to be refined. However, advanced satellite sensors such as SeaWiFS, MODIS, and MERIS enable to measure surface water leaving radiance in six or more wavelengths in the visible spectrum. Therefore, for Case I and Case II waters, Tassan (1994) has elaborated algorithms for estimating chlorophyll, suspended matter, and yellow substance concentrations on the basis of algorithms of estimating chlorophyll concentration in the oceanic waters by Aiken *et*

al. (1995) and Campbell *et al.* (1995). In this thesis advanced optical sensors data from the MODIS sensor was applied in [P2].

However, the ratio of remote observations at two wavelengths is clearly not enough to describe optical properties of absorption and backscattering in natural waters. This means that such ratios used in the above-mentioned retrievals cannot provide detailed information with respect to different affecting optical factors in the natural waters. Therefore, it is necessary to employ multi-spectral information using multivariate regression and neural network algorithms to estimate major water quality variables. This is based on the following reasons:

(1) there is no single spectral channel onboard remote sensors in which the effect of a single absorption (and backscattering) component can be independently dominating on the effect of other water components. On the basis of their spectral absorption and backscattering spectra, it is possible to distinguish some main absorbing and scattering factors such as chlorophyll-a, suspended matter, and yellow substance. However, the fact that several absorbers come into play does not principally prevent solution to the problem (Morel and Prieur 1977);

(2) neural networks with a hidden layer can simulate any complex functions. This means that neural networks are able to model non-linear radiative transfer functions with higher accuracy than those algorithms of traditional regression analyses, although regression methods are still good for linear functions or non-linear transfer functions that are well known (Keiner 1999, Krasnopolsky *et al.* 1995 and 2000).

3. DATA

3.1 Study area

The Gulf of Finland and the coastal archipelago are relatively shallow, with a mean depth of 38 m and a maximum depth of 123 m. The total water volume is about 1,130 km^3. The surface area (29,600 km^2) is small compared with the catchment area (421,000 km^2). The incoming river discharge is about 110 km^3/year. In the easternmost part of the Gulf the salinity is very low because of the fresh water of the River Neva. The average salinity on the surface is close to 6 ‰ in December and 3-6 ‰ in June. The Gulf is also saline stratified and in summer temperature stratified. Figure 3.1 shows the map of the study area.

Figure 3.1: The map of the study area.

The Gulf of Finland is strongly eutrophicated because of the anthropogenic nutrient load. The eutrophication problem of the Gulf has been studied, for example, by Tamminen (1990), Astok *et al.* (1991), Pitkänen *et al.* (1993), and Kuusisto *et al.* (1998). The Gulf receives annually about 9,000 tons of phosphorus and 160,000 tons of nitrogen. Russia, especially the St. Petersburg region, is responsible for most of the nutrient loading. Other important, local loading sources are the Helsinki and Kotka regions in Finland and the coast of the Eastern Viru province and the Tallinn region in

Estonia (Kuusisto *et al.* 1998). All the coastal areas of Finland are at least slightly eutrophicated, but the easternmost part of the Gulf is the most eutrophicated area. In the Finnish coastal areas of the eastern Gulf of Finland, the total phytoplankton biomass of wet weight in the summer is under 2 mg/l, but during the spring peak concentrations can be as much as 30 mg/l (Pitkänen *et al.* 1990). In the Neva estuary the average phytoplankton concentrations are about four to seven times higher than in the western Gulf of Finland (Kauppila *et al.* 1995). Blue-green algae blooms are relatively common in the late summer, but nitrogen fixing from the atmosphere is, however, not very important in the nitrogen cycle of the Gulf (Kononen 1992). In the western Gulf of Finland, nitrogen alone or with phosphorus is the production-limiting nutrient (Pitkänen *et al.* 1990), but the importance of phosphorus grows towards the east. Since nutrients, particularly phosphorus coming from the River Neva and St. Petersburg, are effectively fixed sediments in the Neva estuary (Pitkänen 1991), the estuary is regulating the nutrient conditions in the whole Gulf of Finland. In general, most of the Gulf is nitrogen limited, but the inner Neva estuary is phosphorus limited. Therefore, the factors causing increased light attenuation (phytoplankton, suspended sediment and yellow substance) vary both temporally and spatially.

3.2 In situ data

In situ data were collected concurrently with AISA, Landsat TM and ERS-2 SAR data in August 1997 and with AVHRR and MODIS from April to May 2000, respectively. Water samples at each station (or by ship) were taken from the surface layer of the sea (0-0.5 m). Each year 2-4 smaller motor boats were used for the water sampling. The following water quality variables were measured using the standard methods. Turbidity (FNU-units, EN 27027), Secchi disk depth (transparency), suspended matter (filtered by Nuclepore polycarbonate 0.4 μm), chlorophyll-a (ISO 10260), and water surface temperature, as well as related parameters. All the other laboratory analyses were done at the mainland laboratories of Finnish Environment Institute (SYKE). All samples from the measurement lines were analysed in SYKE within 4-10 hours from sampling (Eloheimo *et al.* 1998), with a view to relating these parameters with the signals in satellite imagery. Ship-borne i*n situ* measurements were conducted from

10:00 am to 17:50 pm on 14th August 1997 by SYKE. 53 *in situ* points data on 14th August 1997 were employed in this thesis. Table 3.1 describes water samples used in the study (53 points) on 14th August 1997.

Table 3.1: Description of water samples used in the study (53 points) on 14.08.1997.

	Minimum	Maximum	Mean	Unit
Chlorophyll-a	2.0	7.7	4.14	μg /l
SSC	1.6	11.0	4.03	mg/l
Turbidity	1.0	7.5	2.59	FNU
SDD	0.67	4.2	2.60	M
SWT	19.2	23.0	20.49	C

Note: SSC means suspended sediment concentration; SDD means Secchi disk depth and SWT means surface water temperature.

During April and May 2000, ship-borne *in situ* measurements were conducted in another way. Water samples were collected from the cooling system of Silja Line ferries and analysed after 14 hours, as started from Helsinki in the afternoon through the Gulf of Finland and coastal archipelago to Stockholm in the next morning. In each ship-borne sampling line, 11 *in situ* data points were made from 19:00 of the previous day to 9:20 of the day. Table 3.2 gives the summary of *in situ* materials for April and May 2000 used in this study.

Table 3.2: The summary of *in situ* data (11 points each date) for April and May 2000.

4Apr	Min	Max	Mean	2May	Min	Max	Mean
Chl-a (μg /l)	1.3	12.0	4.23	Chl-a (μg /l)	2.8	77.0	24.2
Turb(FNU)	0.4	1.1	0.53	Turb(FNU)	0.47	2.7	1.15
WST (C)	0.96	2.83	1.71	WST (C)	3.37	7.26	5.08
10Apr	Min	Max	Mean	8May	Min	Max	Mean
Chl-a (μg /l)	2.1	18.0	8.18	Chl-a (μg /l)	3.8	36.0	18.4
WST(C)	1.23	3.05	1.73	WST(C)	4.34	9.13	5.17
18Apr	Min	Max	Mean	16May	Min	Max	Mean
Chl-a (μg /l)	4.3	15.0	8.81	Chl-a (μg /l)	3.7	38.0	9.94
Turb(FNU)	0.7	8.3	2.14	Turb(FNU)	0.75	3.1	1.38
WST (C)	1.5	4.02	1.92	WST(C)	4.8	11.21	6.0
				22May	Min	Max	Mean
				Chl-a (μg /l)	4.1	32.0	8.48
				WST(C)	5.68	10.55	7.04
				30May	Min	Max	Mean
				Chl-a (μg /l)	3.9	44.0	9.47
				WST(C)	6.7	10.26	7.53

Note: 4Apr means from 19:00 pm on 3rd April to 9:20 am on 4th April 2000; Chl-a means chlorophyll-a; Turb means turbidity; WST means water surface temperature; Turbidity was not available on 10th April, 8th May, 22nd May and 30th May.

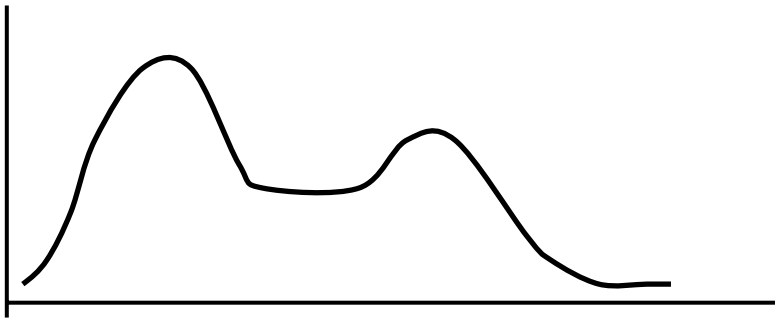

Figure 3.2: The yearly cycle of phytoplankton as a function of time.

Typically, the Gulf of Finland and coastal archipelago freeze during the winter. This leads to the biology of seawater and the evolution of water quality variables to have a roughly repeating yearly cycle (Särkkä 1996, Koponen 2001). Figure 3.2 shows the cycle of the amount of phytoplankton in graphic form.

3.3 Remotely sensed data

In this study, airborne AISA data on 14th August 1997 and space-borne data such as Landsat TM data and ERS-2 SAR data for 16th August 1997 and AVHRR data for 18th April, 21st April, 2nd May, 16th May, 22nd May and 30th May 2000 and MODIS data in April-May 2000 were employed to estimate major water quality variables in the study area. Table 3.3 shows the summary of TM, SAR and AVHRR data used in the study, while AISA and MODIS data are separately introduced later.

Table 3.3: The summary of remotely sensed data used in the study.

Wavelengths	1	2	3	4	5	6	7
TM	0.45-0.52	0.52-0.60	0.63-0.69	0.76-0.90	1.55-1.75	10.4-12.5	2.08-2.35
SAR (cm)	5.3						
NOAA12	0.58-0.68	0.725-1.0	3.55-3.93	10.5-11.5	11.4-12.4		
NOAA14	0.58-0.68	0.725-1.0	3.55-3.93	10.5-11.5	11.4-12.4		

3.3.1 AISA Data

Airborne Imaging Sepectrometer for Applications (AISA) (Mäkisara *et al.* 1993) data were employed in the study. The main characteristics of AISA spectrometer are shown in Table 3.4. Although the total number of AISA channels is 286, the selected

53 channels, for example, covered most of the wavelength range (450-900 nm) were employed during the 1997-1998 campaign.

The AISA data were radiometrically and geometrically corrected and resampled to a pixel size of 2*2 m. To extract 53 channels of AISA data corresponding to those ground truth points (water quality sampling stations), the mean and standard deviation of AISA digital number values were calculated using the defined boxes of 100 by 100 m for each ground truth point.

Table 3.4: Main characteristics of the AISA spectrometer (Mäkisara *et al.* 1993).

Type	Pushbroom CCD-matrix sensor
Number of channels	286
Channel wavelength range	450-900 nm
Channel bandwidth	1.6-9.4 nm (sum of one to six channels)
Number of pixel (across track)	384
Field of view	21^{o}
Pixel size from 1000-m altitude	1 m

3.3.2 Processing of AVHRR data

The Advanced Very-High-Resolution Radiometer (AVHRR) scanning radiometer employs four or five channels. The total field of view is 110.8 degrees centered with nadir (Cracknell 1997). Two satellites in operation make it possible to receive eight images per day at mid-latitudes such as Europe. With a ground resolution of 1.1 km, it cannot replace high-resolution remote sensing satellites. On the other hand, it is possible to make up for the higher spatial resolution with high imaging temporal frequency. The higher temporal frequency makes it possible to get cloud-free imagery for applications involving time series. AVHRR has one visible channel, one near infrared, one mid infrared, and two thermal infrared channels on satellite such as NOAA-12 and -14 (or-15) (see Table 3.3). The benefits from using AVHRR data are imaging with high temporal frequency, relatively low cost, large area coverage, and three thermal infrared channels with absolute calibration (Sucksdorff *et al.* 1997).

In this study, AVHRR data were received by the Finnish Meteorological Institute (FMI) and the AVHRR data from March to August 2000 were checked and pre-processed using AVHRR processing software developed by the Finnish Environment Institute (SYKE). Since *in situ* measurements of water parameters were available

from April to May 2000, a few of them were cloud-free (or partly free) in the Gulf of Finland and have been used to detect turbidity change analysis (Zhang *et al.* 2000). These AVHRR data were also atmospherically and geometrically corrected by SYKE. For the purpose of surface water quality estimation in the Gulf of Finland and coastal archipelago, the digital number (DN) values of AVHRR bands were extracted using the X and Y coordinates corresponding to each ground truth point (same day, but few or more hours later). The spatial size of each grid is 1.1 km*1.1 km.

3.3.3 Processing of MODIS data

In MODIS instrument, two bands are imaged at a nominal resolution of 250 m at nadir, with five bands at 500 m and the remaining 29 bands at 1000 m. A ±55-degree scanning pattern at the EOS orbit of 705 km achieves a 2 330-km swath and provides global coverage every one to two days (http://modis.gsfc.nasa.gov/about/design.html). The two bands of 250-m resolution (620-670 and 841-876 nm), two bands of 500-m resolution (459-479 and 545-565 nm) and nine bands (i.e., centred on 412, 443, 488, 531, 551, 667, 678, 748, 870 nm) of 1000-m resolution at visible and near-infrared (VNIR) wavelengths are suitable for monitoring chlorophyll-a and turbidity in coastal areas (Koponen *et al.* 2002, Zhang *et al.* 2003b).

MODIS data were obtained from GES DAAC archive. For chlorophyll-a estimation in coastal waters of the Gulf of Finland, the bands of 250-m were used to check cloud-covered percentage and nine bands of 1000-m were used to estimate chlorophyll-a in the area. Since *in situ* measurements of chlorophyll-a were available in April and May 2000, a few of MODIS images were cloud-free (or partly free) during April and May 2000 in the Gulf of Finland. In the similar way with AVHRR data extraction, MODIS data were extracted corresponding to those ground truth points by the defined boxes of 1000 by 1000 m for each ground truth point.

3.3.4 Processing methodology for Landsat TM data

Optical/IR satellite remote sensing observations are affected by the atmosphere and radiation from the direct reflectance due to the water surface. These effects should be removed with suitable atmospheric correction and bidirectional reflectance models

before data analysis. When Landsat TM data, transformed into radiances, are used to retrieve quantitative data concerning the water surface, a procedure to correct the measured radiance for the atmosperic contribution is required (e.g., Ouaidrari *et al.* 1999, Zhang and Carder *et al.* 1999). The remaining amount of radiance that reaches the sensor (target radiance) may range from 50% at 450 nm (blue region of electromagnetic spectrum) to 80% at 850 nm (red region) (e.g., Vermote *et al.* 1995, 1997).

According to Equation (2.1), with the hypothesis of homogeneous water reflectance, the radiance energy observed by the Landsat TM sensor consists of several components, and a rough approximation can be expressed as

$$L_{sat} = T_r (L_a + L_u) \tag{3.1}$$

and

$$L_u = L_r + L_w \tag{3.2}$$

where L_{sat} is the radiance received by the TM sensor, and T_r is the atmospheric transmittance due to absorption by atmospheric gases such as ozone, water vapor, carbon dioxide and oxygen. L_a is the atmospheric radiance due to light scattering from gases and aerosols, and L_u is the radiance directly leaving from the water. L_w is the radiance refracted from inside the water body while L_r is the radiance reflected from the water surface. So far, the radiance emitted from the surface of water body itself (L_s) has been ignored.

One approach is to observe a reflectance target such deep clear water as a "dark object" (e.g., Chavez 1988, 1996) that should almost completely absorb all light in the near IR wavelength region, and hence brightness values should be close to zero (e.g., Gilabert *et al.* 1994). Therefore, subtracting constant values from all pixels (“dark pixel” method) does not change statistics of the image. In practice, atmospherically uncorrected data can be used, as operational applications typically require nearly simultaneous in situ data for the calibration. Moreover, the atmospheric correction for case II waters is still a problematic issue and, as a consequence, atmospherically corrected images cannot be either used in retrieval algorithms without supporting reference data. The “dark pixel” method is interesting for coastal waters in cases

where the coastal waters are much more turbid than the clear open sea waters, which is typical e.g. for the Finnish coast line in the Gulf of Finland.

In this study, one scene of Landsat TM data was acquired on 16 August 1997. The resolution of TM data is 30 meters (except band 6 with 120 meters). Since analysis was made for a single image with a quite small angular range, the atmospheric correction does not have a significant effect on correlation analysis. The TM image was geometrically corrected using a land use map (1:25,000) by SYKE, and then the land area of the image was masked off. In order to extract the TM bands data corresponding to 53 ground truth points (water quality sampling stations), the mean and standard deviation of TM digital number values were calculated using 53 defined squares of 300 meters by 300 meters for each ground truth point.

3.3.5 Preliminary assessment of ERS-2 SAR data

The ERS-2 SAR image acquired on 16 August 1997 was pre-processed by European Space Agency (ESA) to the precision image (PRI) level. This means that the image is geometrically correct but orbit-oriented and not registered to any mapping projection system (Populus *et al.* 1995). The pixel size is 12.5 m (but the actual spatial resolution is 25 m) and the coverage is approximately 100 km by 100 km.

The ERS-2 SAR image was geometrically corrected using a land use map (1:25,000) by SYKE, and then the land area of the image was masked off. Similarly to Landsat TM image processing, ERS-2 SAR observations corresponding to 53 ground truth points were also extracted using the same pre-defined squares of a size of 300 meters by 300 meters as in the case of Landsat data.

3.3.6 Data fusion of optical and microwave observations

The key characteristics affecting microwave radar observations, in addition to water dieletric constant, are the water surface roughness properties. Since water mass below the surface does not contribute to the microwave radar backscattering, actual sub-surface water quality characteristics do not directly influence these radar observations.

At optical wavelengths, however, radiation detected by a remote sensing instrument includes both the contribution scattered inside the water body and the contribution reflected from the water surface (see Eq. (3.2)). Therefore, bi-directional reflection of

Sun radiation from the water surface is in the case of optical data merely a factor disturbing the actual water quality retrievals (Zhang *et al.* 1999).

In order to eliminate the effect of incidence/reflection angle variation inside the TM and SAR image, the spatial range in investigations was limited to 60 km (across track range for both images). Moreover, an angular correction was made for SAR signatures (normalization to the incidence angle of 19.5^{o}). This was done due to the strong dependence of water surface backscattering on the angle of incidence, which is evident for ERS-2 SAR data even for as small spatial range as 60 km. The correction was performed by applying an exponential model given by Ulaby *et al.* (1982).

Comparison of nearly simultaneous space-borne optical and microwave observations of a water area was possible on only one occasion, 16th August 1997. On that date, the Landsat TM sensor and the ERS-2 SAR imaged the same coastal region at 8.44 UTC and 9.40 UTC, respectively. Since the time difference between the imaging was less than one hour, the water surface wave conditions, including wind and water temperature, can be assumed to be quite similar for both images (systematic spatial differences in wave conditions). During the previous 24 hours, the average wind speed was about 5.5 m/s with the minimum of 3 m/s and the maximum of 9 m/s. The wind direction was varying from 315^{o} to 360^{o}. The average water surface temperature was about 19.5^{o} C degrees and the average wave height was about 0.39 m with the minimum of 0.2 m and the maximum of 0.8 m (SYKE). Since *in situ* measurements were made on 14th August 1997 and the satellite data were only available on 16th August 1997, we assumed that the water quality conditions were representative for the 16th August 1997 even though the time difference was 2-days (Zhang *et al.* 2003a).

The TM and SAR images had different spatial resolutions and different dynamic ranges of pixel values. The TM imagery had 30 m resolution and 8-bit pixel values whereas the SAR image was provided as 16-bit backscatter intensity values sampled with 25 m ground resolution (Benediktsson and Kanellopoulos 1999). Therefore, in order to use the both images together, it was necessary to co-register and re-sample the data to averaged 300 m resolution.

4. METHODOLOGY

4.1 A semi-empirical algorithm for Secchi disk depth

Secchi disk depth (m), SDD, for monochromatic light is written (Hojerslev 1986) as

$$\mathrm{SDD} = 6.3/c \tag{4.1}$$

where c is the attenuation coefficient (m^{-1}). However, for turbid waters, the contribution to the light attenuation mainly comes from scattering, and thus c is independent of wavelength (Phillips and Kirk 1984). This means that Eq. (4.1) can be considered as a good approximation for the naked eye, without filters (Mulhearn 1995).

Absorption, backscattering and attenuation coefficients (a, b_B and c, respectively) can be further expressed as follows (e.g., Bukata *et al.* 1995)

$$a = a_w + a_{ch} + a_{sm} + a_{ys} \tag{4.2a}$$
$$b_B = 0.5b_w + b_{B\_ch} + b_{B\_sm} \tag{4.2b}$$
$$c = c_w + c_{ch} + c_{sm} + c_{ys} \tag{4.2c}$$

where the subscripts *w, ch, sm, ys* and *B* refer to the contributions from pure sea water, phytoplankton, suspended sediment, yellow substance and backscattering, respectively. Also, $0.5b_w = b_{B\_w,}$ where b_w is the scattering coefficient for pure sea water (Jerlov 1976).

The coastal waters of the Gulf of Finland and the Archipelago Sea is predominantly green to blue-green, except in the plumes of rivers after heavy rain. This means that a submerged Secchi disk can be viewed in a wavelength band similar to that of Landsat TM band 2, i.e., 520-600 nm. Thus, for this band it is reasonable to assume that the effects of yellow substance are negligible (Jerlov 1976). In this band there is a minimum in absorption by phytoplankton (Shifrin 1988). Let us therefore assume that both phytoplankton and suspended sediment are purely scattering centres. That is,

their absorption can be also ignored in this band, i.e., both a_{ch} and a_{sm} are considerably smaller than a_w. Then we can obtain as follows

$$a = a_w \tag{4.3a}$$

$$b_B = 0.5b_w + b_{B\_ch} + b_{B\_sm} \tag{4.3b}$$

$$c = c_w + c_{ch} + c_{sm} \tag{4.3c}$$

The reflectivity, R, is given (Gordon and Morel 1983) by

$$R = 0.33b_B/a \tag{4.4}$$

where R means the ratio of upwelling to downwelling irradiance just below the sea surface, b_B is the backscatter coefficient, and a is the absorption coefficient.

Now, Eq. (4.4) can be written as

$$R = 0.33(0.5b_w + b_{B\_ch} + b_{B\_sm})/a_w \tag{4.5}$$

where R means the reflectivity at the green band (e.g., TM2).

According to Mulhearn (1995) and Bukata *et al.* (1995), let us define the relation between total scatter and backscatter by setting $b_{B\_ch} + b_{B\_sm} = Bb_{ch} + Bb_{sm} = Bc_{ch} + Bc_{sm} = B(c_{ch} + c_{sm})$, where B means the ratio of backscatter to the total scattering coefficient for both phytoplankton and suspended sediment and is assumed to be the same for both of them. Therefore, Eq. (4.5) can also be expressed as

$$R = 0.33(B(c_{ch}+c_{sm})+0.5b_w)/a_w \tag{4.6}$$

From Eq. (4.1) and (4.3c) ($c = c_w + c_{ch} + c_{sm}$), we can obtain

$$c_{ch} + c_{sm} = 6.3/\mathrm{SDD} - c_w \tag{4.7}$$

and then

$$R = 0.33(B(6.3/\mathrm{SDD}- c_w)+0.5b_w)/a_w \tag{4.8}$$

where B is an adjustable constant.

Values quoted in the literature for the ratio of backscatter to the total scattering coefficient for ocean waters, not just for both phytoplankton and suspended matter, i.e., for all particles, range between 0.006 and 0.11 (Mankovskiy 1984, Shifrin 1988). The theoretical value for pure water is 0.5. Values for coastal waters appear to range between 0.006 and 0.025 (Mulhearn 1995). The assumptions in Eq. (4.8) imply that both c_{ch} and c_{sm} are much greater than c_w and that 6.3B/SDD is also much greater than 0.5b_w. Given a value for B of approximately 0.01 and taking c_w = 0.066 m^{-1} and b_w = 0.002 m^{-1} (Hojerslev 1986) for 520-600 nm, both of these assumptions will be satisfied if SDD << 100 m, which is always true in coastal waters.

Thus, Eq. (4.8) can be written as

$$R = 0.33(6.3B/\mathrm{SDD})/a_w \qquad (4.9)$$

and with a_w = 0.064 m^{-1} (Hojerslev 1986),

$$\mathrm{SDD} = 32.5B/R \qquad (4.10)$$

as also obtained by Mulhearn (1995). The semi-empirical algorithm given by Eq. (4.9) and (4.10) assumes that absorption both by yellow substance and by phytoplankton were negligible in the study material. This may cause inaccuracy in SDD retrieval. However, further studies are still needed to refine this semi-empirical algorithm [P1].

4.2 Empirical algorithms for chlorophyll-a

Empirical algorithms in this study include simple regression analysis, multivariate empirical regression analysis, and neural network algorithms. In general, there are two main methods to estimate surface water quality variables. One is the use of empirical algorithms derived from remotely sensed reflectance data. They can provide site-specific predictions of water quality variables with a reasonable accuracy, but are limited in their universal application (e.g., Austin and Petzold 1981, Whitlock *et al.* 1981, Khorram and Cheshire 1985, Gould and Arnone 1997). The other approach is the use of analytic inversion models that require the solution of radiative transfer

equations for deriving absorption and scattering coefficients. The latter approach allows remote sensing measurements to be understood in terms of the inherent optical properties (IOP), and provides insight into the characteristics of the effectiveness and significance of differences in algorithm coefficients in various regions (e.g., Woodruff *et al.* 1999). Although optical properties of the Baltic Sea have been studied (e.g., D'Alimonte *et al.* 2003, Kratzer *et al.* 2003, Darecki and Stramski 2004), I only use empirical methods to retrieve surface water parameters in this study.

For chlorophyll-a retrieval using remote optosensors, regression analysis and empirical neural network methods are applied to estimate chlorophyll-a from AISA, Landsat TM, AVHRR and MODIS data in the study area. The results of chlorophyll-a estimation using these optosensors are also compared. In this study, empirical algorithms for chlorophyll-a (*Chl-a*) from optosensors data can be expressed as

$$Chl\text{-}a = A_0 + A_k \left(\frac{OpticB_i}{OpticB_j} \right)^k \tag{4.11}$$

and

$$Chl\text{-}a = A_0 + \sum A_i (OpticB_i) + \sum A_j ComB_j \tag{4.12}$$

where $OpticB_i$ and $OpticB_j$ can be the digital number (DN) values of optical bands data and $ComB_j$ is the combination of optical bands used in the retrievals (usually used as band ratios or differences). A_0, A_k, A_i, A_j and k are the derived parameters, which can be simulated by using ground truth data [P2].

4.3 Multivariate regression estimation

At the optical wavelengths, the passive remote sensing observations are affected by volume scattering inside the water body and reflection from the water surface. This suggests that all the visible and near-infrared bands can contribute to surface water observations. Therefore, in this study, multivariate regression estimation for major water quality variables (WQV) derived from optical/IR wavelengths is expressed as

$$WQV = A_0 + \sum_{i=1}^{k} A_i (Band)_i \qquad (4.13)$$

where $(Band)_i$ is the digital number (DN) values of visible and near-IR channels of optical satellite data, *k* is the band number of the satellite, and A_0 and A_i are the empirical regression coefficients derived by using the observations from the ground truth points. For instance, *k* is 1 to 7 for Landsat TM data [P1, P3, P5].

Although the passive remote sensing observations are affected by volume scattering inside the water body and reflectance from the water surface, radar signal measurements are only affected by water surface properties other than those in the case of optical/IR observations. However, the temporal and spatial variations in water surface roughness are actually factors that disturb the interpretation of optical data (e.g., Lindell *et al.* 1999). Therefore, it may be possible to develop empirical algorithms using both optical data and radar data to estimate surface water quality parameters.

In this case study, multivariate empirical retrievals for major water quality variables (WQV) derived from combined optical data and microwave data can be expressed as

$$WQV = A_0 + \sum_{i=1}^{k} A_i (Band)_i + B(SAR) \qquad (4.14)$$

where $(Band)_i$ is the digital number (DN) values of visible and near-IR channels of optical satellite data, *k* is the band number of the satellite, *SAR* is the DN values of SAR intensity, and A_0 , A_i and *B* are the empirical regression coefficients derived by using observations from the ground truth points [P1, P3, P5].

4.4 A neural network algorithm

In this study, a neural network algorithm was applied to estimate surface water quality parameters using both optical and microwave data. In coastal waters, the presence of suspended sediments and dissolved organic matter creates an optically complex situation (Bukata *et al.* 1991, Keiner and Yan 1998). Therefore, the task of modelling

the transfer function seems a natural application for a neural network. The network is a combination of neurons designed to solve a certain problem. The network has at least three layers: input layer, a hidden layer and output layer (Figure 4.1). This neural network is a so-called feed-forward network and is typically used in function approximation application. All information moves in one direction during operation, from the input layer to the output layer. The first layer distributes the input parameters (usually radiance measurements at different wavelengths in case of optical remote sensing) to the second layer. The second layer (also called hidden layer) consists of a varying number of neurons, where each input parameter is multiplied by its connection's weight and all the inputs to the neuron are summed and passed through the non-linear sigmoid function. The third layer receives the output of the second layer in which it is processed through neurons again (Keiner 1999).

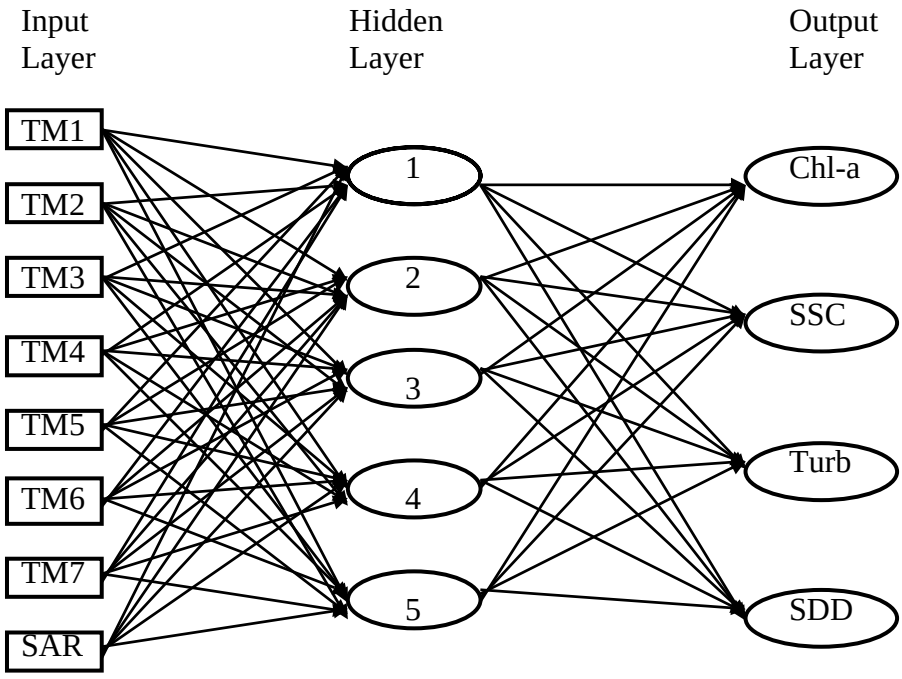

Figure 4.1: A neural network diagram in this study.

A neural network can model a large number of non-linear behaviors, yet without prior knowledge of the nature of non-linearity. Standard linear regression does not model non-linear relationships properly, while non-linear regression requires having a priori knowledge of the nature of the non-linear behavior. However, a neural network does not have such limitations. Therefore, the neural network is most useful when

applied in situations where the data is non-linear or chaotic, or if the required signal is deeply hidden within noise or other signals (Masters 1993, Krasnopolsky *et al.* 1995 and 2000, Keiner 1999).

In a neural network, each neuron has two parts: a linear summation function and a non-linear activation function. Figure 4.2 presents a neuron with *n* inputs. The inputs to each neuron are firstly routed through the summation function. The output of this function inside the neuron at node *j* is given by

$$y_j = \sum_{i=1}^{n} w_{ij} x_i + b_j \tag{4.15}$$

where x_i are the inputs, w_{ij} are the weights related to each input/node connection, and b_j is the bias related to node *j*, and y_j is the output of this function inside the neuron at node *j*. The inputs to the neuron are multiplied by their associated weights, summed and added to the bias. The weights control which inputs and connections in the network are more important than others. The bias controls the activation level of neuron, when the resulting sum is passed through a non-linear activation function

$$z_j = g(y_j) = \tanh(y_j) = \tanh(\sum_{i=1}^{n} w_{ij} x_i + b_j) \tag{4.16}$$

where *g* is a sigmoid activation function and z_j is the output of hidden layer after the non-linear summation. The activation function is what gives the network its ability to model non-linear behavior (Krasnopolsky *et al.* 1995 and 2000, Keiner 1999).

In this study, the inputs are the digital values from all channels of TM and one channel of ERS-2 SAR. The values from the input layer are distributed to the five nodes in the hidden layer, where the summation and activation functions are performed. The output values of the hidden layer are then the input values of the network's output layer, which also performs the summation and activation functions. The output of this layer is the values of the geophysical variables

$$Y = a \tanh\left(\sum_{k=1}^{j} w_k z_k + b\right) \qquad (4.17)$$

where Y is the vector of geophysical variables, w_k is the weight between the hidden layer and the output layer, b is the bias related to the output layer, and j is the number of nodes in the hidden layer. The output is scaled by the factor a, which is used in the training network and it depends on the output range of variables. Before the training network, the variables should be scaled into (0, 1). It is proven that a neural network with one hidden layer can simulate any complex functions (Keiner 1999). This is known as the Kolmogorov representation theorem (Beale and Jackson 1990, Masters 1993).

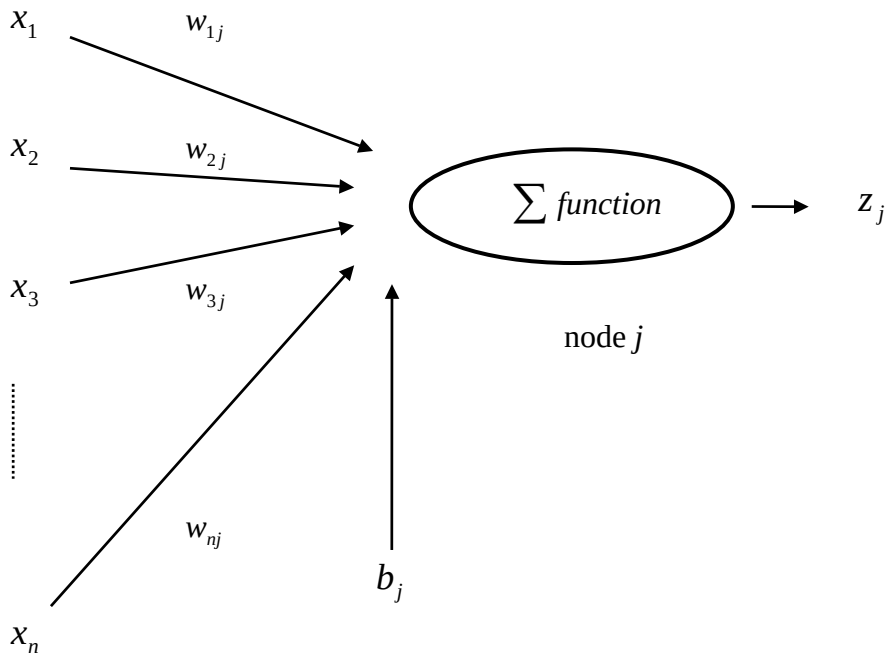

Figure 4.2: A neuron at node j.

The number of hidden layer nodes depends on the complexity of the approximated function. Although enough nodes in the network can simulate the function correctly, too many nodes will result in increased training time and possible overfitting. The overfitting is a case where the network correctly learns not only the correct model, but also the noise in the inputs, resulting in a poor application to a real problem (Krasnopolsky *et al.* 1995, Keiner 1999). Based on experimentation, five hidden layer nodes were used to model the transfer function correctly from all channels of TM and

one channel of SAR to selected parameters of surface water quality in the test region. The weights related to each connection were also randomly created before training.

In this case study, the network was trained using Matlab Neural Network Toolbox. The error minimum for each trial was calculated using the Levenberg-Marquardt line-minimization method (Beale and Jackson 1990). In order to determine the optimal number of hidden nodes, the training was performed with 7 TM bands and 1 SAR channel data as input, and the number of hidden nodes varying from 2 to 10 here. The output of the network was compared to the *in situ* measurements of surface water quality variables, including chlorophyll-a, suspended sediment concentration, turbidity, and Secchi disk depth. However, for the output of water surface temperature, the input used only TM band 6 and SAR. The root mean square error (*RMSE*) and regression (R^2) of the comparison were calculated. For each number of hidden nodes, the training process was run 2-20 times with random initial weights. The weight configuration that returned the smallest error was retained for validation [P1, P3, P4, P5].

In a similar way, this neural network algorithm was also applied to estimate some major surface water quality variables using AVHRR and MODIS data from April to May 2000 [P2, P6].

5. RESULTS AND DISCUSSION

In this section, the results and comparison of employed algorithms are described using AISA, Landsat TM and ERS-2 SAR data for August 1997, as well as AVHRR and MODIS data from April to May 2000 to estimate major surface water variables in the Gulf and coastal archipelago of Finland.

5.1 Simple regression and correlation analyses

The results from the simple regression analysis of chlorophyll-a (Chl-a), suspended sediment concentration (SSC), turbidity (Turb), and Secchi disk depth (SDD), in relation to Landsat TM data and ERS-2 SAR data, are presented in Table 5.1 [P4].

Table 5.1: Correlation (R^2) between Chl-a, SSC, ln(SSC), Turb, and SDD with ratios, logarithmic transformations and combinations of TM bands and SAR data.

	TM1	*TM2*	*TM3*	*TM4*	*TM5*	*TM6*	*TM7*	*ERS-2*	*TM1/2*
Chl-a	0.024	0.003	0.026	0.019	0.020	0.012	0.008	0.357	0.198
SSC	0.376	0.467	0.533	0.284	0.057	0.007	0.032	0.098	0.226
ln(SSC)	0.339	0.459	0.503	0.245	0.043	0.003	0.022	0.090	0.284
Turb	0.476	0.626	0.664	0.391	0.044	0.019	0.023	0.055	0.323
SDD	0.204	0.383	0.530	0.460	0.164	0.064	0.073	0.368	0.354
	TM1/3	*TM1/4*	*TM2/1*	*TM2/3*	*TM2/4*	*TM3/1*	*TM3/2*	*TM3/4*	*TM4/1*
Chl-a	0.322	0.129	0.204	0.239	0.005	0.358	0.263	0.017	0.215
SSC	0.253	0.067	0.236	0.139	0.231	0.327	0.164	0.406	0.058
ln(SSC)	0.276	0.070	0.299	0.125	0.260	0.359	0.148	0.420	0.050
Turb	0.292	0.085	0.362	0.121	0.313	0.400	0.136	0.497	0.080
SDD	0.537	0.007	0.411	0.382	0.071	0.651	0.416	0.291	0.005
	TM4/2	*TM4/3*	*TM3-4*	*TM2-4*	*TM2+3*	*ln(TM1)*	*ln(TM2)*	*ln(TM3)*	*ln(TM4)*
Chl-a	0.039	0.006	0.025	0.002	0.007	0.071	0.0001	0.021	0.023
SSC	0.175	0.345	0.534	0.465	0.493	0.280	0.371	0.464	0.256
ln(SSC)	0.191	0.367	0.506	0.458	0.478	0.255	0.377	0.461	0.224
Turb	0.258	0.428	0.661	0.622	0.646	0.391	0.528	0.603	0.370
SDD	0.043	0.245	0.516	0.374	0.429	0.116	0.265	0.460	0.442
	TM1/(1+2+3)	*TM2/(1+2+3)*	*TM3/(1+2+3)*	*TM1/(1+2+4)*	*TM2/(1+2+4)*	*TM4/(1+2+4)*	*TM2/(2+3+4)*	*TM3/(2+3+4)*	*TM4/(2+3+4)*
Chl-a	0.272	0.111	0.363	0.251	0.165	0.119	0.251	0.246	0.018
SSC	0.281	0.156	0.292	0.213	0.257	0.117	0.039	0.219	0.224
ln(SSC)	0.337	0.215	0.304	0.273	0.319	0.118	0.029	0.202	0.242
Turb	0.383	0.263	0.317	0.317	0.380	0.171	0.091	0.199	0.312
SDD	0.498	0.227	0.616	0.404	0.380	0.006	0.230	0.471	0.079

Note: *Chl-a = Chlorophyll-a, SSC = Suspended sediment concentration, Turb = Turbidity, SDD = Secchi disk depth, ERS-2 = ERS-2 SAR, TM1/2 = TM1/TM2, TM3-4 = TM3-TM4, TM1/(1+2+3) = TM1/(TM1+TM2+TM3) etc.*

Chlorophyll-a is only weakly correlated with all TM bands (less than 0.100). All visible and near-IR bands (Bands 1-4) were significantly predictive of turbidity with the exception of the TM5, TM6 and TM7. Variations in turbidity were most adequately explained by TM3, which explained 66.4% of the variation in a significant regression. These same bands were also significantly predictive of variations in SDD and SSC, although no single variable explained more than 53.3% of these two variations. However, ERS-2 SAR explained 35.7% and 36.8% for chlorophyll-a and SDD respectively, while SAR only explained 5.5% of the variation in turbidity and 9.8% of the variation in SSC.

The algorithms developed in this study were also combined with those of band ratios, band differences, logarithmic transformations, chromaticity analyses and some other possible combinations of visible and near-IR bands (TM 1-4) to find the best one for comparison (see Table 5.1). The most successful combination for chlorophyll-a was a linear equation of together using TM2, TM4, (TM2-TM3)/TM1, and TM4/(TM1+TM2+TM4) with the coefficient of determination (R^2 = 0.677) and the error in the dependent parameter estimate (that is, root mean square error RMSE = 0.958 μg /l). The best combination for suspended sediment concentration was using TM1, TM2, and TM3 together in a linear equation with the coefficient of determination (R^2 = 0.542) and the error in the dependent parameter estimate (RMSE = 1.465 mg/l). The most successful combination for turbidity was using TM1, TM3, TM1/TM3, and (TM3-TM4)/TM2 together in a linear equation with the coefficient of determination (R^2 = 0.690) and the error in the dependent parameter estimate (RMSE = 0.817 FTU). The best combination for Secchi disk depth was using TM1, TM2, and TM3 together in a linear equation with the coefficient of determination (R^2 = 0.724) and the error in the dependent parameter estimate (RMSE = 0.454 m) (Zhang *et al.* 1999, Zhang *et al.* 2000a).

An examination of the correlation (R^2) between turbidity and chlorophyll-a for August 1997 showed values as low as 0.066. This suggested that the turbidity in the Gulf of Finland was not dependent on plankton biomass in the used data set (Zhang *et al.* 1998). However, the correlation of turbidity with suspended sediment concentration (SSC) is up to 0.815, which implies that turbidity is significantly related to suspended sediments in the Gulf. In contrast, SDD has a correlation (R^2) of 0.312

with chlorophyll-a and that of 0.493 with SSC. This means that SDD is weakly, but significantly correlated to both dissolved and particulate organic matter in the study. Material examination of the correlations (R^2) between observed intensities at different TM bands ranged from 0.001 to 0.933 (Table 5.2). This difference among TM bands implies that they may either change significantly at any site or change differently at all sites. This may also have a significant effect on the results of data analysis. However, the high relationship between TM bands probably means that these bands are measuring similar aquatic properties in the study.

Table 5.2: Correlation (R^2) matrix of Landsat TM bands [P3].

	TM1	*TM2*	*TM3*	*TM4*	*TM5*	*TM6*
TM2	*0.890*					
TM3	*0.797*	*0.933*				
TM4	*0.356*	*0.454*	*0.567*			
TM5	*0.030*	*0.047*	*0.108*	*0.504*		
TM6	*0.018*	*0.052*	*0.081*	*0.133*	*0.088*	
TM7	*0.034*	*0.030*	*0.062*	*0.264*	*0.654*	*0.001*

Table 5.3 shows the correlations (R^2) between the ERS-2 SAR derived backscattering coefficient and different TM channels. The results indicate that the data from visible bands of TM are to a degree correlated with the C-band ERS-2 SAR observations. The highest correlation (R^2) of 0.144 is between SAR data and TM band 2 (TM2). Since angular corrected SAR observations are only dependent on the surface wave conditions (in addition to random speckle, which was mostly averaged out in the employed water area signatures), this suggests that systematic variations in wave conditions in different parts of TM image caused 14.4% of the total variability in TM2 observations (see Figure 5.1) (Zhang *et al.* 2002a).

Table 5.3: Correlation (R^2) between Landsat TM bands and ERS-2 SAR data at coastal regions (archipelago) of Finland on 16 August 1997 (661 points).

	TM1 *(450-520nm)*	*TM2* *(520-600nm)*	*TM3* *(630-690nm)*	*TM4* *(760-900nm)*	*TM5* *(1550-1750nm)*	*TM6* *(10450-12500nm)*	*TM7* *(2080-2350nm)*
ERS-2	*0.109*	*0.144*	*0.129*	*0.029*	*0.000*	*0.012*	*0.019*

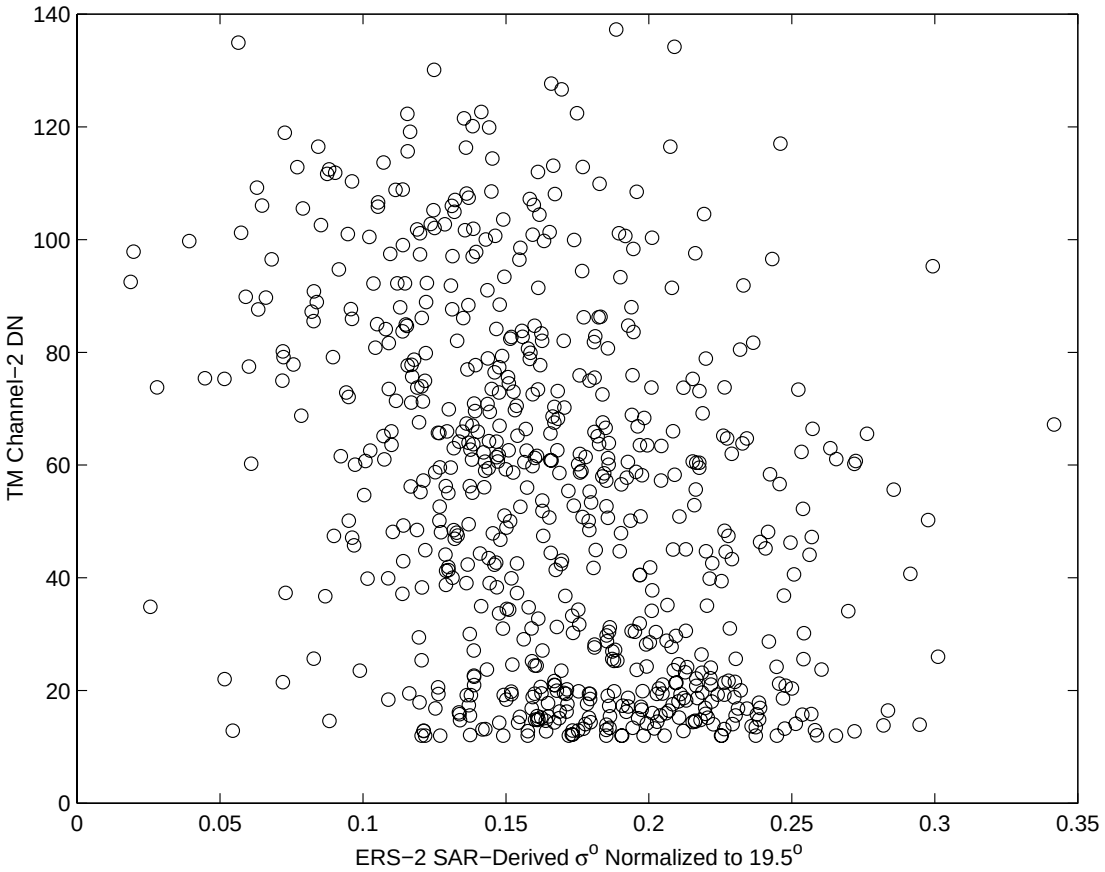

Figure 5.1: Behavior of observed TM2 intensity as a function of observed C-band ERS-2 SAR backscattering coefficient (R^2 =0.144) (661 points) (Eloheimo *et al.* 1997, Zhang *et al.* 2002a).

The results from simple regression analysis indicate that these water quality variables can be estimated using single-band Landsat TM and ERS-2 SAR data, but the estimated accuracy is relatively low that it is not practically sufficient to monitor water quality characteristics in the study area. However, this method is useful to find good relationships with single bands, band ratios, and their combinations in the area.

5.2 A semi-empirical algorithm for Secchi disk depth

Using Eq. (4.10), SDD derived from TM2 is plotted against the measured SDD in Fig. 5.2. For this algorithm, the coefficient of determination is R^2 = 0.521, the root mean square error is RMSE = 0.681 m, and the adjustable constant B = 0.0167.

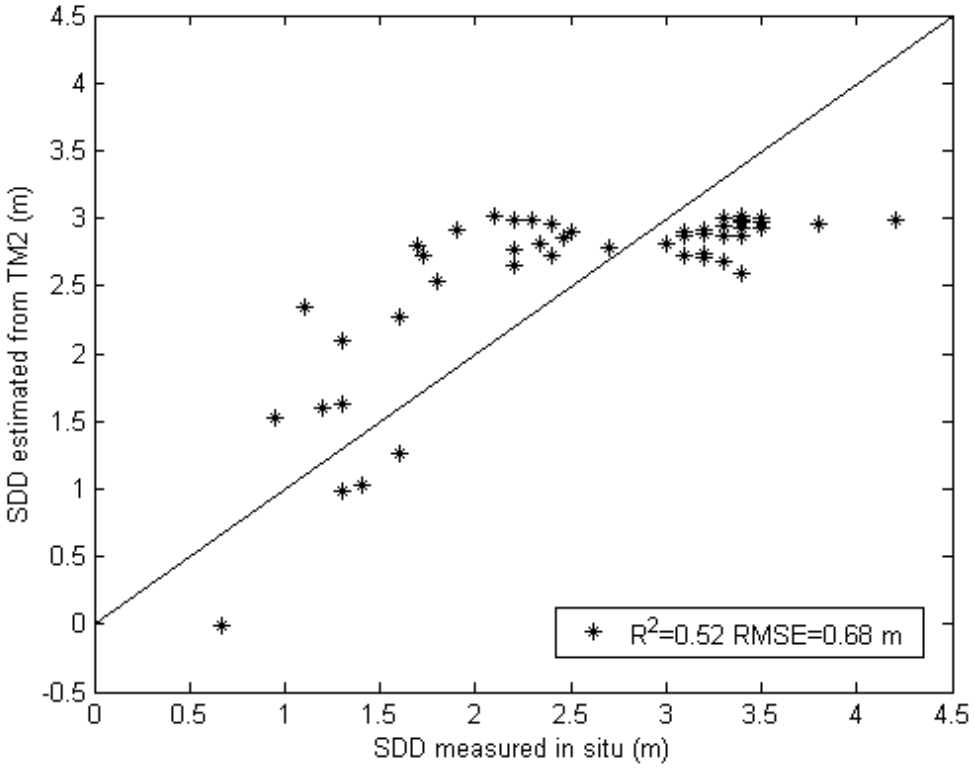

Fig. 5.2: Regression of SDD estimated from TM2 with the measured SDD using the semi-empirical algorithm [P1].

Clearly, this result is not as good as expected to retrieve SDD in the coastal waters of the study area. The main reason is that the absorption by yellow substance and by phytoplankton was assumed to be negligible in the semi-empirical algorithm [P1]. However, this semi-empirical algorithm is not recommended in the area.

5.3 Empirical algorithms for chlorophyll-a

5.3.1 Chlorophyll-a estimation from AISA data

Chlorophyll-a is adequately retrieved from AISA data using only the band ratio. In the study, the following relation was used to estimate chlorophyll-a from Eq. (4.11)

$$Chl-a = -72.9973 + 98.5510\left(\frac{L_{\lambda=687nm}}{L_{\lambda=674nm}}\right) \qquad (5.1)$$

with the regression determination coefficient (R^2 =0.872) and the root mean square error (*RMSE* = 0.550 $\mu g / l$). Clearly, AISA data of high spatial and spectral resolutions with its narrow bandwidth is adequate to estimate chlorophyll-a in the study area with satifactory accuracy. However, the drawback is the high cost and a large dataset [P2].

5.3.2 Chlorophyll-a estimation from MODIS data

MODIS data were available for 21st April and 16th May 2000. Nine channels at the central wavelengths of 412 nm, 443 nm, 488 nm, 531 nm, 551 nm, 667 nm, 678 nm, 748 nm and 870 nm were used to estimate chlorophyll-a. The most successful combination in the area for the chlorophyll-a retrieval from MODIS data using equation (4.12) was

$$Chl-a = 5.1372 - 0.0025(L_{\lambda=488nm}) - 0.0027(L_{\lambda=748nm}) - 130.6416(ComB_1) + 136.1009(ComB_2) \quad (5.2)$$

where $ComB_1 = \frac{L_{\lambda=667nm}}{L_{\lambda=551nm}}$ and $ComB_2 = \frac{L_{\lambda=678nm}}{L_{\lambda=531nm}}$ with the regression determination coefficient (R^2 =0.761) and the root mean square error (*RMSE* = 0.855 $\mu g / l$). This retrieval accuracy is satisfactory for estimating chlorophyll-a in the study area [P2].

5.4 Multivariate regression algorithms using TM and SAR data

5.4.1 Suspended sediment concentrations

Suspended sediment concentration (SSC) was estimated by using various independent variables in regression algorithms in this study. Using digital number (DN) values of all TM bands and ERS-2 data, SSC can be estimated applying Eq. (4.13) and (4.14)

$$SSC = 8.6880-0.0221(TM1)-0.0202(TM2)+0.2831(TM3)-0.2822(TM4) +0.3639(TM5)-0.0405(TM6)-0.2579(TM7) \quad (5.3)$$

with the coefficient of determination R^2 = 0.572 and with the root mean square error RMSE = 1.416 mg/l or, as ERS-2 SAR is also employed

$$SSC = 7.0587-0.0084(TM1)-0.085(TM2)+0.2181(TM3)-0.1592(TM4) \\ -0.2518(TM5)-0.0394(TM6)-0.2416(TM7)+0.0033(SAR) \quad (5.4)$$

with the coefficient of determination R^2 = 0.578 and RMSE = 1.406 mg/l. The latter regression explained 57.8% of the variation in SSC with an RMSE of 1.406 mg/l. These results show that SSC derived using all TM 7 bands together with ERS-2 SAR data slightly improves the retrieval accuracy. The summary of SSC estimated from combined different TM bands and ERS-2 SAR data as well as the comparison with those from different TM bands data is presented in Table 5.4.

Table 5.4: The summary of suspended sediment concentration (SSC) derived from TM bands and from combined TM/ERS-2 SAR data (53 points).

	SUSPENDED SEDIMENT CONCENTRATION (SSC)										
ALGORITHM	TM1	TM2	TM3	TM4	TM5	TM6	TM7	SAR	A_0	R^2	RMSE
Eq. (4.1), k=7	-0.0221	-0.0202	0.2831	-0.2822	0.3639	-0.0405	-0.0257	-	8.6880	0.572	1.416
Eq. (4.2), k=7	-0.0084	-0.0085	0.2181	-0.1592	0.2518	-0.0394	-0.2416	0.0033	7.0587	0.578	1.406
Eq. (4.1), k=4	-0.0146	-0.0225	0.2662	-0.3199	-	-	-	-	2.4308	0.545	1.460
Eq. (4.2), k=4	-0.0004	-0.0074	0.1953	-0.3034	-	-	-	0.0035	0.7543	0.552	1.449
Eq. (4.1), k=3	-0.0135	-0.0166	0.2243	-	-	-	-	-	1.7594	0.542	1.465
Eq. (4.2), k=3	0.0009	-0.0015	0.1635	-	-	-	-	0.0035	0.0795	0.549	1.454

Note: R^2 = Regression, RMSE = Root mean square error

The results indicate that the variation of SSC is more significantly correlated to visible bands than to near-IR bands of TM data. This demonstrates that optical characteristics in this case study are dominated by absorption from both dissolved and particulate organic matter. As a result, the reflectance increases more rapidly at the visible region than at near-IR region due to the backscattering by suspended matter.

These results also show that the combined SAR data and TM bands data have not improved the SSC retrieved accuracy in our case study. This is expected as Table 5.1 indicates that ERS-2 SAR data has a very low correlation (R^2 =0.098) with SSC. The results suggest that the additional use of SAR only improves SSC estimation slightly in this study.

Although the algorithms used in other similar studies as well as some other possible combinations were tested, none of these algorithms improved the SSC estimation accuracy in this case study (see Table 5.1). A probable reason is that the coastal waters in the Gulf of Finland and coastal archipelago are optically dominated by absorption and backscattering from both dissolved and particulate organic matter [P3]. However, this method is not recommended in the area due to a low accuracy.

5.4.2 Chlorophyll-a concentrations

The correlation of TM 7 bands with chlorophyll-a shows weak relationships (see Table 5.1). The chlorophyll-a level may change substantially from day to day so that the correlations of TM bands with chlorophyll-a were much lower than with other parameters such as turbidity.

Chlorophyll-a (CHL) was derived using various independent variables in multivariate algorithms in this study. Using digital number values of all TM bands and SAR data, CHL can be derived applying Eq. (4.13) and (4.14)

$$CHL = 15.1329-0.1573(TM1)+0.0394(TM2)+0.2671(TM3)-0.5383(TM4) +0.1214(TM5)-0.0606(TM6)+0.1007(TM7) \quad (5.5)$$

with the coefficient of determination R^2 = 0.542 and with the root mean square error RMSE = 1.144 μg /l or, as ERS-2 SAR is also employed

$$CHL = 13.1451-0.1405(TM1)+0.0537(TM2)+0.1878(TM3)-0.3882(TM4) -0.0153(TM5)-0.0593(TM6)+0.1206(TM7)+0.0040(SAR) \quad (5.6)$$

with the coefficient of determination R^2 = 0.556 and with the root mean square error RMSE = 1.126 μg /l.

The summary of chlorophyll-a retrievals from combined different TM bands and ERS-2 SAR data as well as the comparison with those from TM bands data only is presented in Table 5.5.

Table 5.5: The summary of chlorophyll-a (*CHL*) derived from combined TM/SAR data (53 points).

	Chlorophyll-a (*CHL*)										
ALGORITHM	TM1	TM2	TM3	TM4	TM5	TM6	TM7	SAR	A_0	R^2	RMSE
Eq. (4.1), k=7	-0.1573	0.0394	0.2671	-0.5383	0.1214	-0.0606	0.1007	-	15.1329	0.542	1.144
Eq. (4.2), k=7	-0.1405	-0.0537	0.1878	-0.3882	-0.0153	-0.0593	0.1206	0.0040	13.1451	0.556	1.126
Eq. (4.1), k=4	-0.1359	0.0265	0.2455	-0.5702	-	-	-	-	7.6481	0.413	1.295
Eq. (4.2), k=4	-0.1173	0.0463	0.1523	-0.5485	-	-	-	0.0045	5.4427	0.433	1.273
Eq. (4.1), k=3	-0.1341	0.0369	0.1887	-	-	-	-	-	6.4515	0.396	1.314
Eq. (4.2), k=3	-0.1150	0.0570	0.0947	-	-	-	-	0.0035	4.2230	0.417	1.291

Note: R^2 = Regression, RMSE = Root mean square error

The results show that the accuracy of chlorophyll-a derived from these multivariate retrievals using TM bands combined with SAR data is slightly higher than that from TM bands alone in the study. This is expected as Table 5.1 indicated that SAR data has a low but significant correlation (R^2=0.357) with chlorophyll-a. This may suggest that SAR data is helpful for retrieving chlorophyll-a in the area. In other words, it may means that either (a) high chlorophyll-a contents cause smoothening of the water surface or (b) high chlorophyll-a contents occur in regions where water surface is smooth [P5]. However, this small improvement is marginal in the area.

5.4.3 Turbidity and Secchi disk depth

Turbidity and Secchi disk depth (SDD) are both optical measurements of water quality and, therefore, differ from suspended sediment concentration for example,

which is a measure of the weight of inorganic particulates suspended in the water column (e.g., Harrrington and Schiebe 1992).

Multivariate regression algorithms for turbidity and SDD showed differences in either variable selection or statistical quality. Therefore, using the digital number values of 7 TM bands and single-channel ERS-2 data according to Eq. (4.13) and (4.14), turbidity (*Turb*) can be derived by

$$Turb = 4.1106-0.0346(TM1)+0.0294(TM2)+0.1123(TM3)+0.5137(TM4) \\ -0.2775(TM5)-0.0204(TM6)-0.0324(TM7) \quad (5.7)$$

with the coefficient of determination R^2 = 0.709 and with the root mean square error RMSE = 0.794 FNU.

As ERS-2 SAR data is used in addition to TM data we obtain

$$Turb = 4.1024-0.0346(TM1)+0.0294(TM2)+0.1120(TM3)+0.5143(TM4) \\ -0.2781(TM5)-0.0204(TM6)-0.0323(TM7)+0.0000(SAR) \quad (5.8)$$

with the coefficient of determination R^2 = 0.709 and with RMSE = 0.794 FNU. Both of these regressions explained 70.9% of the variation with a root mean square error (RMSE) of 0.794 FNU. The results show that the turbidity algorithm derived using combined 7 TM bands together with ERS-2 SAR is same as that using TM data only. This suggests that the SAR data does not improve the turbidity retrieval accuracy in this case study.

The summary of multivariate turbidity algorithms from combined TM/ERS-2 data as well as the comparison with those from different TM bands is presented in Table 5.6. The results indicate that visible bands provide the greatest ability for estimating turbidity variations using Landsat TM data. These results also demonstrate that the accuracy of turbidity estimation using combined TM bands and ERS-2 SAR data is not higher than that using TM bands, or only a marginal contribution to turbidity retrievals if using combined visible TM bands and ERS-2 SAR data. This is expected as Table 5.1 indicates that the SAR data has a very low correlation (R^2 =0.055) with turbidity. This probably means that turbidity is not significantly affected by the water

surface properties in the study [P3]. However, the multivariate regression method using optical remote sensing data to estimate turbidity is recommended in the area.

Table 5.6: The summary of turbidity (*Turb*) derived from TM bands and from combined TM/ERS-2 SAR data (53 points).

	TURBIDITY (Turb)										
ALGORITHM	TM1	TM2	TM3	TM4	TM5	TM6	TM7	SAR	A_0	R^2	RMSE
Eq. (4.1), k=7	-0.0346	0.0294	0.1123	0.5137	-0.2775	-0.0204	-0.0324	-	4.1106	0.709	0.794
Eq. (4.2), k=7	-0.0346	0.0294	0.1120	0.5143	-0.2781	-0.0204	-0.0323	0.0000	4.1024	0.709	0.794
Eq. (4.1), k=4	-0.0305	0.0367	0.0952	0.0636	-	-	-	-	0.6909	0.681	0.830
Eq. (4.2), k=4	-0.0325	0.0345	0.1054	0.0612	-	-	-	-0.0005	0.9338	0.682	0.829
Eq. (4.1), k=3	-0.0307	0.0355	0.1015	-	-	-	-	-	0.8245	0.681	0.830
Eq. (4.2), k=3	-0.0328	0.0333	0.1119	-	-	-	-	-0.0005	1.0699	0.682	0.830

Note: R^2 = Regression, RMSE = Root mean square error

Secchi disk depth (SDD) was estimated using algorithms with various independent variables. Therefore, by using Eq. (4.13) and (4.14), SDD can be derived by

$$SDD = 1.8780+0.0427(TM1)+0.0017(TM2)-0.1419(TM3)-0.2562(TM4) +0.0185(TM5)+0.0085(TM6)+0.0054(TM7) \quad (5.9)$$

with the coefficient of determination R^2 = 0.740 and RMSE = 0.441 m or, as ERS-2 SAR data is also applied

$$SDD = 3.4515+0.0294(TM1)-0.0097(TM2)-0.0791(TM3)-0.3750(TM4) +0.1268(TM5)+0.0074(TM6)-0.0104(TM7)-0.0031(SAR) \quad (5.10)$$

with the coefficient of determination R^2 = 0.774 and RMSE = 0.412 m. The latter regression explained 77.4% of the variation in SDD with a root mean square error (RMSE) of 0.412 m. The results show that the accuracy of SDD using combined TM/ERS-2 is slightly higher than that of using TM bands (74% of the variation with

an RMSE of 0.441 m). This implies that SDD is to some degree correlated to the surface water properties in this study. The summary of SDD derived from combined different TM bands and ERS-2 SAR data as well as the comparison with those from different TM bands data is presented in Table 5.7.

Table 5.7: The summary of Secchi disk depth (SDD) derived from TM bands and from combined TM/ERS-2 SAR data (53 points).

	SECCHI DISK DEPTH (SDD)										
ALGORITHM	TM1	TM2	TM3	TM4	TM5	TM6	TM7	SAR	A_0	R^2	RMSE
Eq. (4.1), k=7	0.0427	0.0017	-0.1419	-0.2562	0.0185	0.0085	0.0054	-	1.8780	0.740	0.441
Eq. (4.2), k=7	0.0294	-0.0097	-0.0791	-0.3750	0.1268	0.0074	-0.0104	-0.0031	3.4515	0.774	0.412
Eq. (4.1), k=4	0.0404	0.0017	-0.1374	-0.1898	-	-	-	-	3.0962	0.731	0.449
Eq. (4.2), k=4	0.0283	-0.0112	-0.0768	-0.2039	-	-	-	-0.0030	4.5298	0.763	0.421
Eq. (4.1), k=3	0.0410	0.0052	-0.1563	-	-	-	-	-	2.6979	0.724	0.454
Eq. (4.2), k=3	0.0291	-0.0073	-0.0982	-	-	-	-	-0.0029	4.0762	0.755	0.429

Note: R^2 = Regression, RMSE = Root mean square error

These results indicate that the variation in SDD is more significantly correlated with visible bands than with near-IR bands of TM data. Since the Gulf of Finland is optically dominated by absorption from both dissolved and particulate organic matter, the reflectance increases more rapidly at the visible region than at near-IR region due to the backscattering by suspended matters. Although the coefficient to SAR in algorithms is quite close to zero (i.e., -0.0031), the retrieved SDD is slightly higher than that using the coefficient as zero in the study. The results also show that the accuracy of SDD estimated from combined TM/ERS-2 data is slightly better than that from TM bands. This is expected as Table 5.1 indicates that ERS-2 SAR data has to some extent correlation (R^2 =0.368) with SDD. The results suggest that SAR data is slightly helpful for estimating SDD in this study [P1]. In fact, this small improvement is marginal in the study area. The multivariate regression method using optical remote sensing data to estimate SDD is recommended in the area.

5.4.4 Water surface temperatures

The correlation of TM 7 bands with water surface temperature (WST) shows weak relationships as in Table 5.8. Probably, Landsat TM6 (10.4-12.5 μm) may be affected by the atmospheric water vapour that absorbs radiation in the 8-12 μm wavelengths, and also the TM6 may include both emitted infrared radiation and reflected solar infrared radiation during the daytime.

Using the quadratic regression (Baban 1993), the WST was estimated by using the digital number values of Landsat TM band 6

$$WST = 36.3409-0.2613(TM6)+0.0010(TM6)^2 \quad (5.11)$$

with the coefficient of determination R^2 = 0.157 and RMSE = 0.814^0 C.

Table 5.8: Correlation coefficient (R^2) between Landsat TM bands and water surface temperature (WST) at the coastal archipelago of Finland on 16 August 1997.

	TM1	*TM2*	*TM3*	*TM4*	*TM5*	*TM6*	*TM7*	*SAR*
WST	0.021	0.085	0.165	0.158	0.061	0.131	0.025	0.291

Water surface temperature (WST) was estimated using various independent variables in multivariate algorithms in this study. Using digital number values of all TM bands and SAR data, WST can be derived applying Eq. (4.13) and (4.14)

$$WST = 18.1489-0.0393(TM1)-0.0191(TM2)+0.1486(TM3)+0.1660(TM4) \\ -0.4037(TM5)+0.0172(TM6)+0.2151(TM7) \quad (5.12)$$

with the coefficient of determination R^2 = 0.436 and with the root mean square error RMSE = 0.666^0 C or, as ERS-2 SAR is also employed

$$WST = 16.6320-0.0265(TM1)-0.0081(TM2)+0.0881(TM3)+0.2805(TM4) \\ -0.5018(TM5)+0.0182(TM6)+0.2303(TM7)+0.0030(SAR) \quad (5.13)$$

with the coefficient of determination R^2 = 0.466 and RMSE = 0.648 ^{0}C. The latter regression explains 46.6% the variation in water surface temperature with an RMSE of 0.648 ^{0}C.

The result from Equation (5.11) demonstrates that Landsat TM6 (10.4-12.5 μm) not only includes emitted infrared radiation and reflected solar infrared radiation during the daytime, but also is significantly affected by the atmospheric water vapour that absorbs radiation in the 8-12 μm wavelengths. On the other hand, the results using Equations (5.12) and (5.13) of multivariate regression algorithms improved the SWT retrieval to some extent from that obtained with Equation (5.11). Although the correlation coefficients between SWT and TM1, TM2, TM5 and TM7 are close to zero (see Table 5.8), the retrieved SWT using the coefficients of these bands as zero is less than that using all TM bands data in the study. The result also shows that the WST estimated by using all TM 7 bands combined with SAR data improves the retrieval accuracy. This is expected as Table 5.8 indicates that the SAR data has some correlation (R^2 = 0.291) with WST. This probably suggests that the SAR data has some supplementary values to TM data for the WST retrieval in this study.

These results demonstrate that the retrievals of major water quality variables using multivariate empirical algorithms are better than those using simple regression analyses. This suggests that multi-spectral data may include more information of water characteristics in the study. However, the multivariate regression algorithms still need to be refined for the practical use in the area.

5.5 Empirical neural network estimation using TM and SAR data

The developed empirical neural network algorithms are quite different in the selected bands when compared with those used in other studies (e.g., Lindell *et al.* 1985, Lathrop and Lillesand 1986, Tassan 1987, Lathrop *et al.* 1991, Lavery *et al.* 1993, Pattiaratchi *et al.* 1994, Keiner and Yan 1998). This is because the different types of phytoplankton and sediments affect the optical properties of the water at different geographical sites. In order to indicate the significance of the regression models, the coefficient of determination (R^2) and root mean square error (RMSE) have been calculated. The results also indicate that SAR has some contribution to the estimation

of some major parameters, if these parameters are correlated to water surface properties (see Table 5.9).

Table 5.9: Comparison of regression analysis and neural network estimation.

	Regression analysis		*Neural network*	
	TM	TM+SAR	TM	TM+SAR
	Chl-a		***Chl-a***	
R^2	0.542	0.556	0.903	0.923
RMSE	1.144 μg /l	1.126 μg /l	0.526 μg /l	0.467 μg /l
	SSC		***SSC***	
R^2	0.572	0.578	0.888	0.908
RMSE	1.416 mg/l	1.406 mg/l	0.723 mg/l	0.654 mg/l
	Turb		***Turb***	
R^2	0.709	0.709	0.942	0.963
RMSE	0.794 FNU	0.794 FNU	0.351 FNU	0.280 FNU
	SDD		***SDD***	
R^2	0.740	0.774	0.916	0.951
RMSE	0.441 m	0.412 m	0.249 m	0.191 m
	WST		***WST***	
R^2	0.436	0.466	0.858	0.875
RMSE	0.666 ^0C	0.648 ^0C	0.333 ^0C	0.313 ^0C

These statistical results, however, show that regression analysis is poor to characterize the relationship between both the digital data of TM and SAR and the water quality parameters in this case study. The main reason is the poor ability of regression analysis to model the unknown non-linear transfer function (Keiner and Yan 1998) in surface waters. Although regression can be used to model well for linear or known non-linear transfer functions, a linear regression algorithm cannot estimate the relationship adequately between *in situ* measurements and satellite observations in the Gulf and coastal archipelago of Finland.

The neural network was trained using one group of sub-datasets (27 points data) for surface water quality parameters, including chlorophyll-a (Chl-a), suspended sediment concentration (SSC), turbidity (Turb), Secchi disk depth (SDD), and water surface temperature (WST) using Landsat TM and ERS-2 SAR data on 16th August 1997. Table 5.9 gives the statistics for the comparison between the results using the neural network and using linear regression analysis. R^2 and *RMSE* for the neural network were calculated in the same way as in the case of regression analysis. Figure 5.3 shows an example of turbidity for R^2 and *RMSE* values of the validation data set (i.e., the other group of sub-datasets, 26 points data) as a function of the number of hidden layer neurons. It is clear that the estimation accuracy increases with the

increasing number of hidden nodes. Using the validation data set, 5 hidden nodes for each input are good enough in our study [P4].

The *RMSE* for estimation results using the neural network algorithms were about 11.2% for chlorophyll-a, 15.2% for suspended sediment concentration, 11.2% for turbidity, 7.3% for Secchi disk depth and 1.6% for water surface temperature, which are significantly better than those of regression analysis, 23.1%, 35.9%, 32.8%, 16.5%, and 3.3% respectively [P4]. The graphical comparisons between the results of regression analysis and the neural network are shown in Figure 5.4, Figure 5.5, Figure 5.6, Figure 5.7 and Figure 5.8 respectively for chlorophyll-a, suspended sediment concentration, turbidity, Secchi disk depth and water surface temperatures. These results clearly indicate that the performance of the neural network is substantially better than the performance of regression algorithms. This is expected because of the non-linear nature of the transfer function between the surface water characteristics and satellite remote sensing observations.

The results of this study also support those of the other previous results (e.g., Leivuori and Vallius 1998). The 1-10 mg/l concentration of suspended sediments shown in Figure 5.5 for the Gulf of Finland does not really limit the phytoplankton growth. However, the small spatial correlation ($R^2 = 0.04$) between chlorophyll-a and suspended sediment concentration and the presence of high sediment/low chlorophyll-a concentration (Figure 5.9) suggest that the limiting factor at that time was the availability not of nutrients but of light, which can be observed in higher concentrations of suspended sediments in the study area (see Fig. 5.9).

Although some other studies have used the general correlation between chlorophyll-a and suspended sediment concentration in coastal waters to substitute the observations of suspended sediments as chlorophyll-a, it seems that the results in this study do not support this method. On the other hand, turbidity is always used as a proxy for suspended sediment concentration in the Gulf of Finland. Secchi disk depth is another major parameter used in the study area because it has a good correlation with both chlorophyll-a and suspended sediments. Furthermore, water surface temperature is one of other major parameters in surface waters. The neural network algorithm, however, appears to estimate these major parameters in surface waters independently of the relationship to each other.

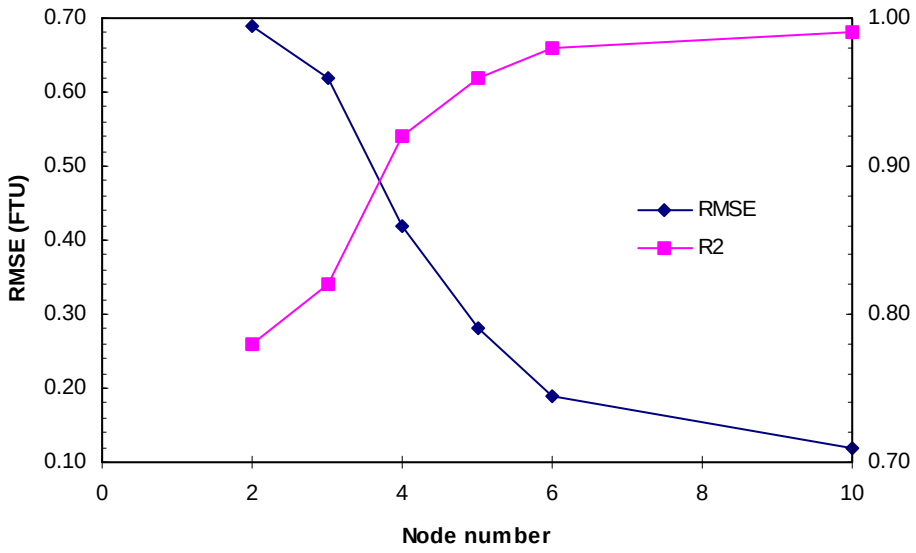

Figure 5.3 Turbidity RMSE and R^2 for the neural network as a function of the number of hidden nodes

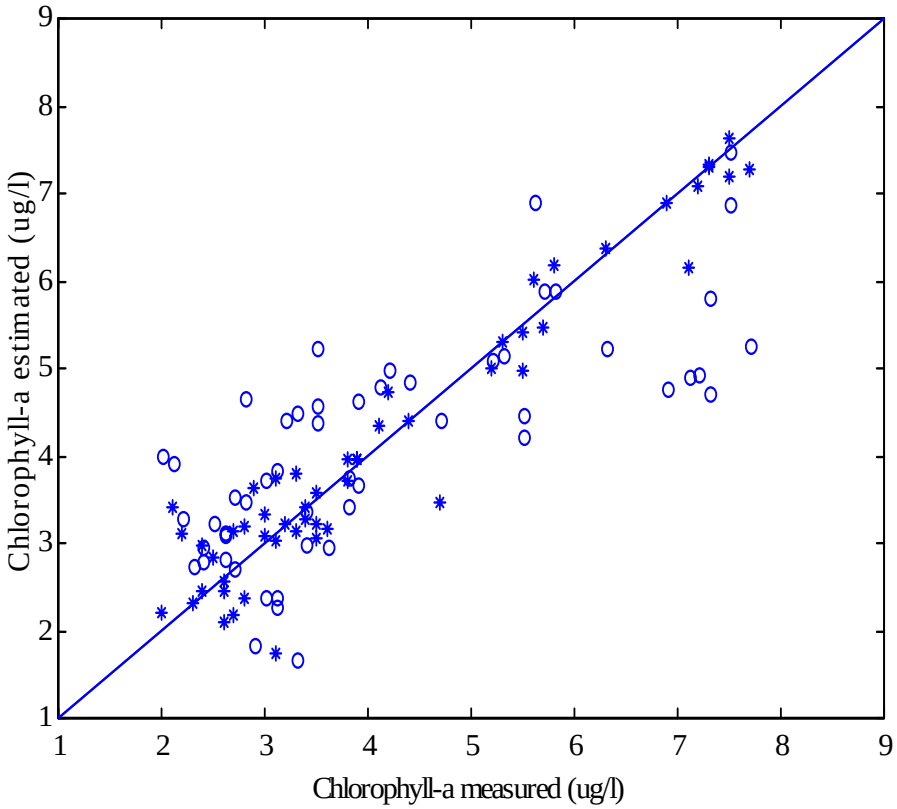

Figure 5.4 Comparison of results from regression analysis (o) and neural network (*) for chlorophyll-a estimation

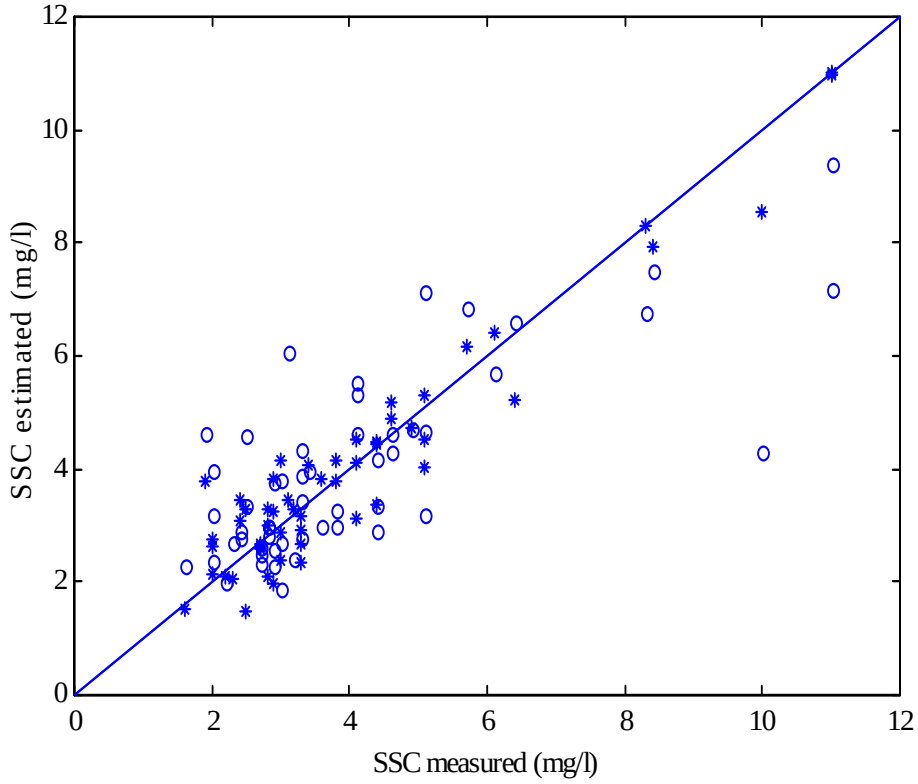

Figure 5.5 Comparison of results from regression analysis (o) and neural network (*) for suspended sediment concentration (SSC) estimation

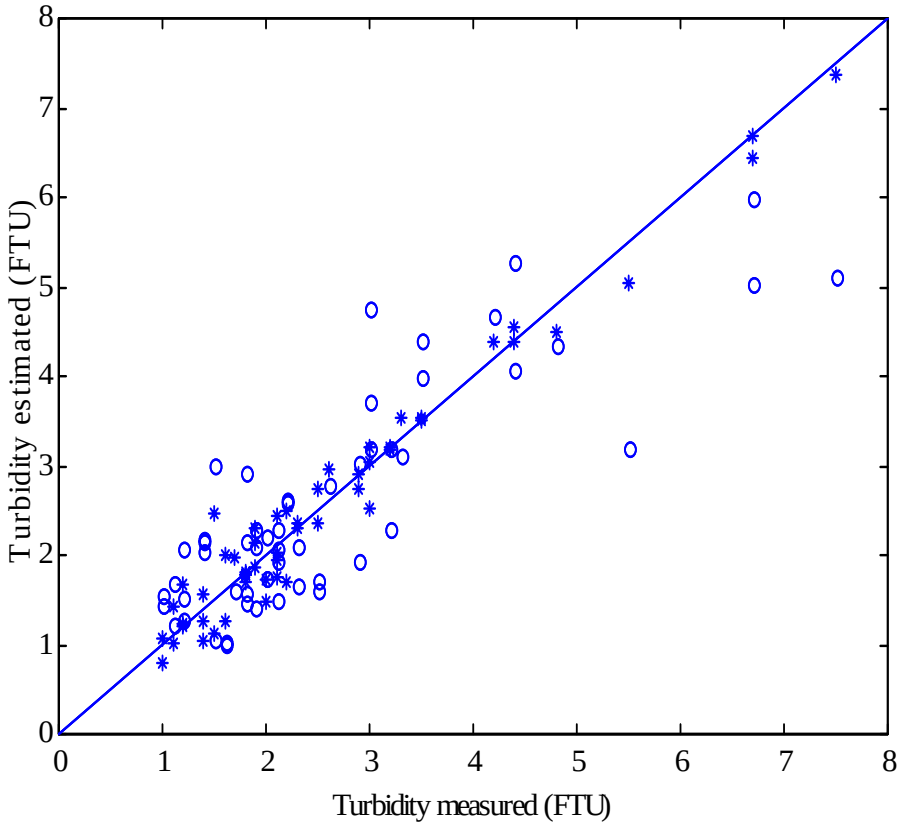

Figure 5.6 Comparison of results from regression analysis (o) and neural network (*) for turbidity estimation

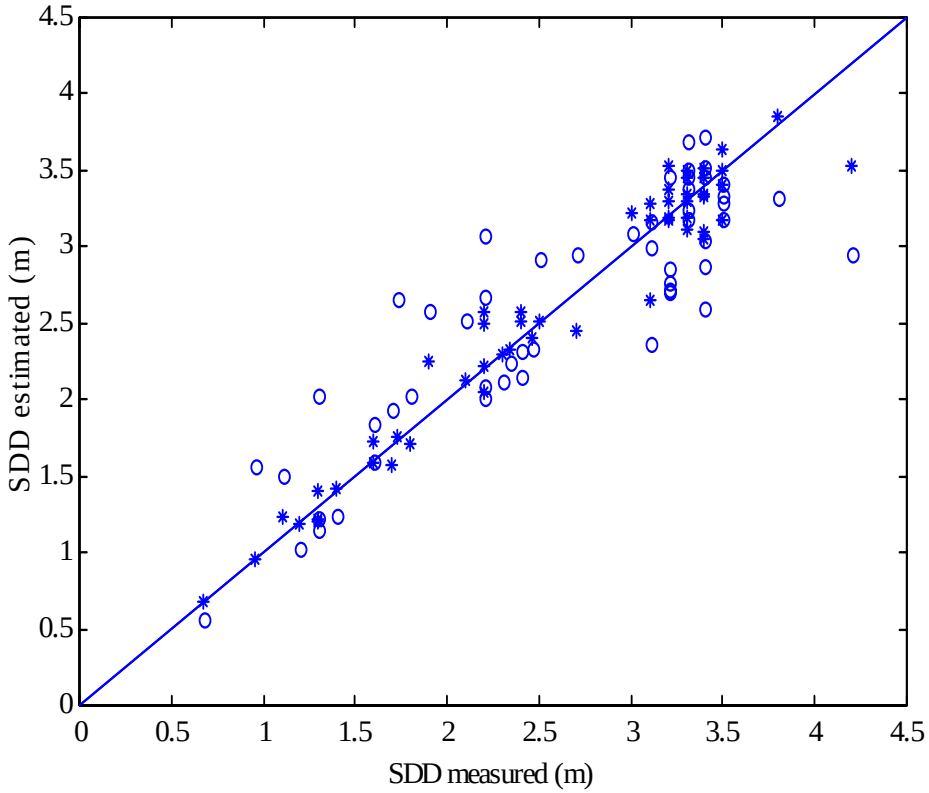

Figure 5.7 Comparison of results from regression analysis (o) and neural network (*) for Secchi disk depth (SDD) estimation

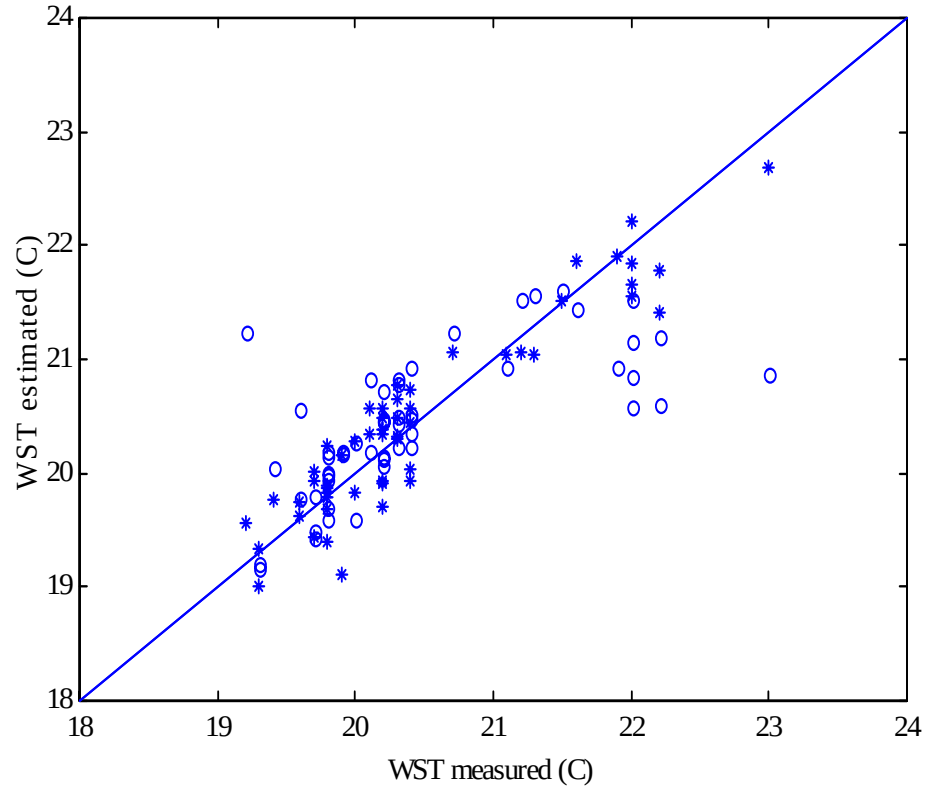

Figure 5.8 Comparison of results from regression analysis (o) and neural network (*) for water surface temperature (WST) estimation

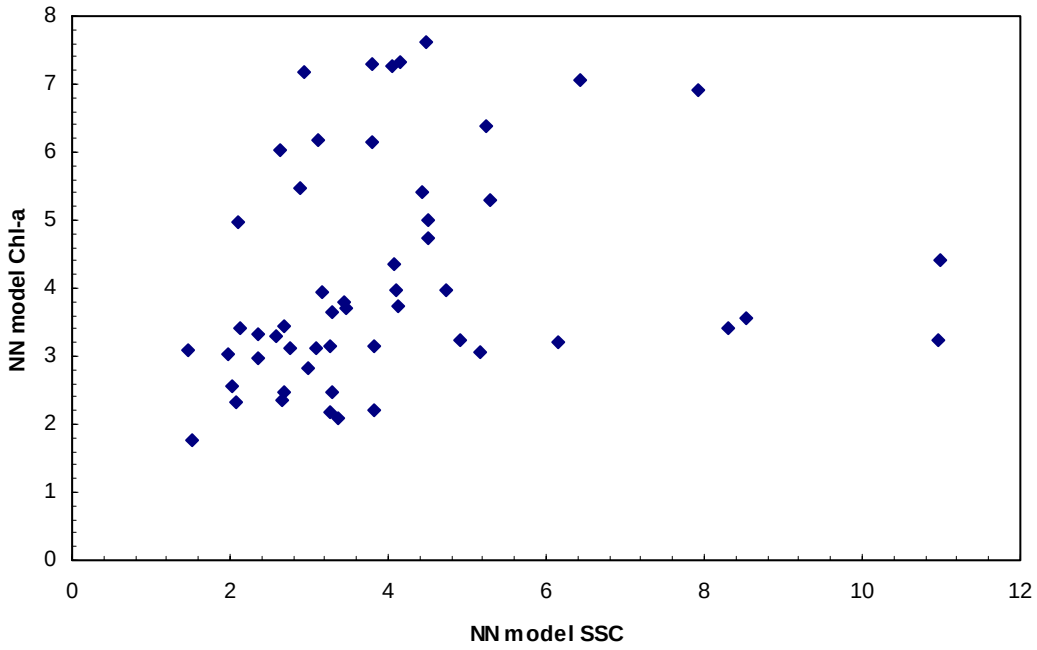

Figure 5.9 A relationship plot of chlorophyll-a (μg /l) estimated and suspended sediment concentration (mg/l) estimated by neural network.

The methodology presented in this study can be applied to other coastal waters where remote sensing of surface water quality information is important. The neural network algorithms of surface water quality approximation should also be applied to present and near-future sensors such as MODIS and MERIS. Multi-temporal use of satellite remote sensing for the estimation of major parameters in surface waters will permit to determine seasonal and yearly cycles and trends in coastal waters such as in the Gulf of Finland.

5.6 Empirical estimation using AVHRR data

AVHRR data have widely been applied to detect changes in environmental studies. In this study, I present empirical algorithms of AVHRR data to estimate major water quality variables in the Gulf of Finland and Finnish archipelago. Both AVHRR data and *in situ* measurements are available for April and May 2000. In the study, however, AVHRR data for 18th and 21st April employed the same *in situ* measurements on 18th April available in empirical algorithms, while there were no AVHRR close to *in situ* measurements of 4th April, 10th April and 8th May. In each

ship-borne line sampled 11 *in situ* data points from 19:00 pm of the previous day to 9:20 am of the day. Table 5.10 gives the summary of AVHRR and *in situ* materials used in this study.

Table 5.10: The summary of AVHRR and *in situ* materials (11 samples) in this study.

In situ points (11)	AVHRR	Day-difference
Chl-a, Turb, WST (18April)	3data (16, 17, 18April)	2daysdiff
Chl-a, Turb, WST (18April)	1data (21April)	3daysdiff
Chl-a, Turb, WST (2May)	3data (1May, 2May, 3May)	1daydiff
Chl-a, Turb, WST (16May)	1data (18May)	2daysdiff
Chl-a, WST (22May)	3data (21May, 22May, 23May)	1daydiff
Chl-a, WST (30may)	3data (29May, 30May, 31May)	1daydiff

Note: 18April means 18th April 2000; Chl-a means chlorophyll-a; Turb means turbidity; WST means water surface temperature; 2daysdiff means 2-days difference between AVHRR data and *in situ* measurements; 3data means three dates of AVHRR data.

5.6.1 Simple regression and correlation analyses

Simple regression analyses for chlorophyll-a (Chl), turbidity (Turb), and water surface temperature (WST), in relation to AVHRR in April and in May 2000, are presented in Table 5.11 and Table 5.12, respectively. Both chlorophyll and turbidity have better correlations using the difference of Band 1 and Band 2 (B1-2) than the single Band 1 and/or Band 2. The highest correlation is of R^2 = 0.720 between chlorophyll and the difference of B1-2, while the highest correlation is of R^2 = 0.702 between turbidity and the difference of B1-2 on 2nd May 2000. Therefore, this result strongly supports the results from previous studies such as Woodruff *et al.* (1999) to estimate turbidity using AVHRR data. However, the WST has a higher relationship (R^2 = 0.545) with the difference of Band 4 and Band 5 (B4-5) than the single Band 4 and/or Band 5 on 18th April, while the WSTs of other five data sets have less relationships with the difference of B4-5 than the single Band 4 and/or Band 5. This may be caused by the different date acquisitions of AVHRR data used in the study. Fig. 5.10 shows an example of turbidity detection using the simple empirical algorithm from AVHRR data on 21st April 2000.

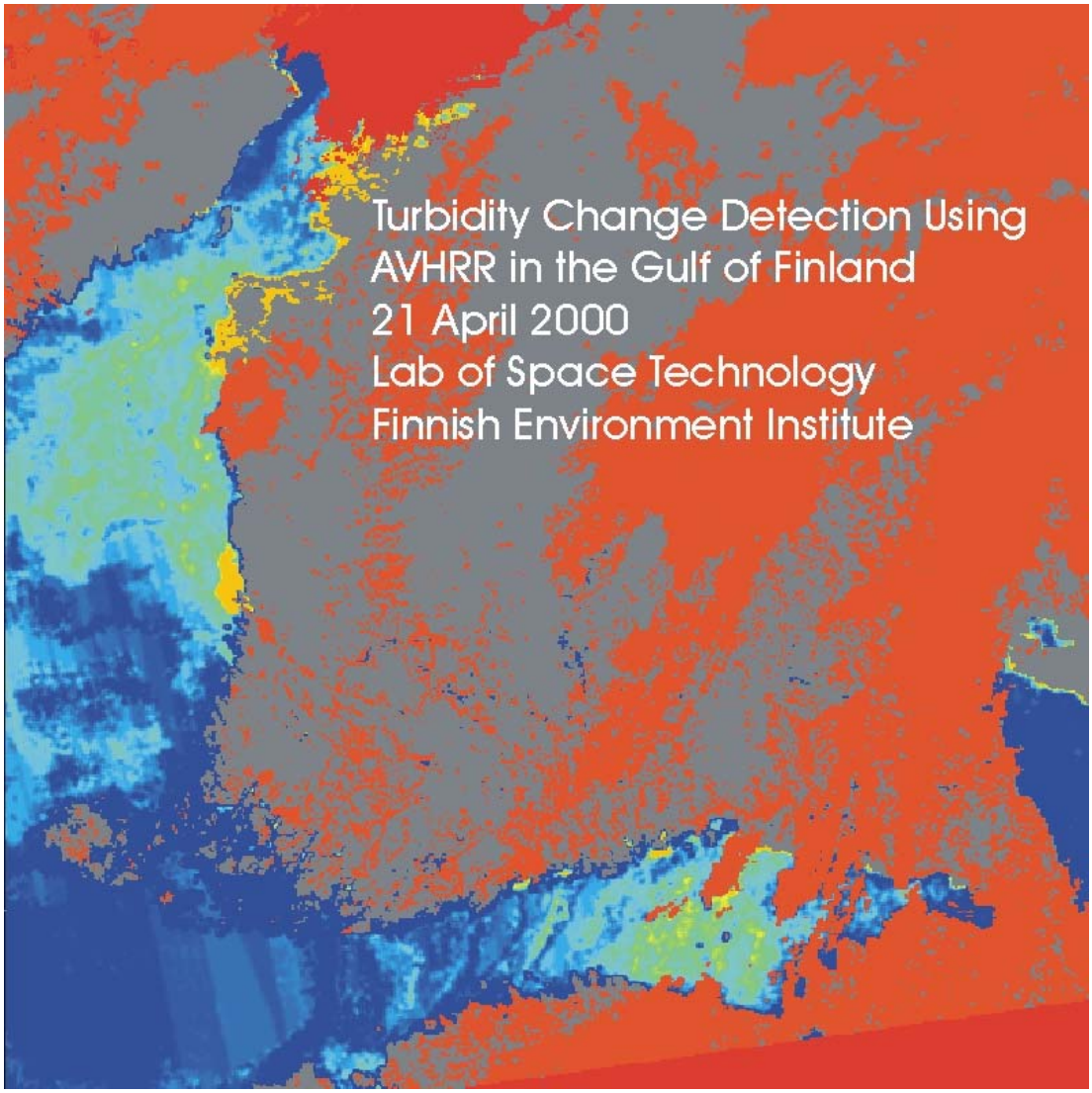

Figure 5.10: Turbidity detection using AVHRR imagery in the Gulf of Finland and Gulf of Bothnia.

Table 5.11: Correlations (R^2) of water quality variables with AVHRR bands and band differences in April 2000.

	Apr 18	Apr 18	Apr 18	Apr 21	Apr 21	Apr 21
	CHL	Turb	WST	CHL	Turb	WST
B1	0.051	0.003	0.000	0.049	0.242	0.000
B2	0.102	0.002	0.003	0.031	0.140	0.015
B3	0.219	0.074	0.077	0.005	0.056	0.022
B4	0.049	0.327	0.079	0.027	0.805	0.531
B5	0.009	0.072	0.017	0.064	0.806	0.423
B1-2	0.237	0.295	0.104	0.115	0.595	0.409
B4-5	0.227	0.421	0.545	0.141	0.154	0.092

Note: CHL=Chlorophyll-a, Turb=turbidity, WST=Water surface temperature, B1=Band1 etc., B1-2=Band1-Band2, B4-5=Band4-Band5, Apr18=April 18 etc.

Table 5.12: Correlations (R^2) of water quality variables with AVHRR different bands and band differences in May 2000.

	May 02			*May 16*			*May 22*		*May 30*	
	CHL	Turb	WST	CHL	Turb	WST	CHL	WST	CHL	WST
B1	0.344	0.410	0.389	0.029	0.009	0.000	0.000	0.011	0.028	0.019
B2	0.338	0.411	0.403	0.057	0.001	0.008	0.000	0.004	0.030	0.030
B3	0.254	0.321	0.348	0.080	0.000	0.038	0.049	0.015	0.003	0.005
B4	0.613	0.641	0.596	0.235	0.321	0.316	0.101	0.214	0.005	0.346
B5	0.601	0.618	0.537	0.136	0.248	0.259	0.086	0.213	0.003	0.288
B1-2	0.720	0.702	0.795	0.310	0.041	0.011	0.009	0.121	0.106	0.003
B4-5	0.016	0.028	0.098	0.185	0.042	0.019	0.115	0.043	0.018	0.157

Note: CHL=Chlorophyll-a, Turb=turbidity, WST=Water surface temperature, B1=Band1 etc., B1-2=Band1-Band2, B4-5=Band4-Band5, May02= May 02 etc.

An examination of the correlation (R^2) between water quality variables such as chlorophyll-a, turbidity and water surface temperature in April and May 2000 is presented in Table 5.13. The results indicate that turbidity has higher correlations with chlorophyll-a in May (R^2=0.880 and R^2=0.789) than those in April (R^2=0.043 and R^2= 0.008). This may suggest that the turbidity in the study area was significantly dependent on plankton biomass in May, whereas it was slightly dependent on plankton biomass in April in the used data set [P2, P6].

Table 5.13: Correlations (R^2) of water quality variables in April and May 2000 (11 points for each ship-sampling line).

	Apr 04	Apr 04	Apr 10	Apr 18	Apr 18		
	CHL	Turb	CHL	CHL	Turb		
Turb	0.043			0.008			
WST	0.066	0.109	0.345	0.013	0.537		
	May 2	May 2	May 8	May 16	May 16	May 22	May 30
	CHL	Turb	CHL	CHL	Turb	CHL	CHL
Turb	0.880			0.789			
WST	0.296	0.568	0.241	0.453	0.279	0.130	0.019

Note: CHL=Chlorophyll-a, Turb=turbidity, and WST=Water surface temperature

Material examination of the correlations (R^2) between observed intensities at different AVHRR channels (bands) of April and May 2000 are presented in Table 5.14 and Table 5.15. Due to cloudy weather AVHRR images were not available for all the dates of *in situ* measurements. Hence, AVHRR data with a max three-days difference to the dates of *in situ* measurements were also checked and employed to estimate major water quality variables used in the study (see Table 5.10). Table 5.14

shows that the correlations of AVHRR five bands on 18th April ranged from 0.002 to 0.967 and on 21st April ranged from 0.051 to 0.974. Table 5.15 shows that the correlations of AVHRR bands on 2nd May ranged from 0.016 to 0.982, on 16th May from 0.151 to 0.992, on 22nd May from 0.051 to 0.991, and on 30th May from 0.002 to 0.996. These differences among AVHRR bands imply that these bands may either change significantly at any site or change differently at all sites. This may also have a significant effect on the results of data analysis.

The results from a simple regression analysis indicate that these water quality variables can be detected using the band difference of Band1 and Band2 of AVHRR data, but the estimated accuracy is too low to monitor water quality characteristics in the area. However, simple regression method is recommended to find relationships of AVHRR bands with water quality parameters in the area.

Table 5.14: Correlations (R^2) of AVHRR bands in April 2000 available.

	Apr 18				*Apr 21*			
	B1	B2	B3	B4	B1	B2	B3	B4
B2	0.967				0.965			
B3	0.852	0.889			0.872	0.951		
B4	0.003	0.002	0.013		0.228	0.116	0.051	
B5	0.016	0.004	0.008	0.774	0.289	0.159	0.075	0.974

Note: B1=Band1, B2=Band2, B3=Band3, etc.,

Table 5.15: Correlations (R^2) of AVHRR bands in May 2000 available.

	May 02				*May 16*			
	B1	B2	B3	B4	B1	B2	B3	B4
B2	0.982				0.992			
B3	0.693	0.679			0.860	0.867		
B4	0.028	0.040	0.058		0.151	0.125	0.142	
B5	0.016	0.023	0.053	0.973	0.275	0.247	0.259	0.949
	May 22				*May 30*			
	B1	B2	B3	B4	B1	B2	B3	B4
B2	0.991				0.996			
B3	0.217	0.203			0.683	0.684		
B4	0.281	0.241	0.111		0.029	0.025	0.005	
B5	0.210	0.184	0.051	0.915	0.009	0.007	0.002	0.971

Note: B1=Band1, B2=Band2, B3=Band3, etc.

5.6.2 Multivariate regression algorithms using AVHRR data

Chlorophyll-a (CHL) was derived using various independent variables in multivariate algorithms in our study. Using digital number values of AVHRR all 5 bands for April 18, 2000, for example, CHL can be estimated applying Equations (4.13)

$$CHL = 43.5979-5.8544(B1)+6.7506(B2)-0.0321(B3) +0.1625(B4)-0.2675(B5) \quad (5.14)$$

with the coefficient of determination R^2 = 0.624 and with the root mean square error RMSE = 2.577 μg /l.

The summary of chlorophyll-a retrievals from AVHRR bands is presented in Table 5.16. The results show that the accuracy of chlorophyll-a derived from multivariate retrievals using AVHRR bands is better than those from simple regression analyses in the case study. This suggests that all AVHRR bands provide more information of chlorophyll-a concentration than what a single AVHRR band does in the area [P2].

Table 5.16: The summary of chlorophyll-a retrievals from AVHRR bands.

CHL	*B1*	*B2*	*B3*	*B4*	*B5*	A_0	R^2	*RMSE*
Apr18	-5.8544	6.7506	-0.0321	0.1625	-0.2675	43.5979	0.624	2.577
Apr21	-6.7658	7.2397	-0.1368	-1.4295	1.4309	31.4208	0.407	6.001
May02*	0.0013	-0.0008	-0.0010	0.0040	0.0086	-3.1533	0.885	6.237
May16	-0.5657	0.5458	0.5153	1.6702	-0.3126	-512.522	0.808	2.268
May22	-0.0330	0.0303	0.0042	0.0386	-0.0182	-62.0479	0.543	1.046
May30	0.0752	-0.0731	-0.0063	0.3109	-0.3363	91.2915	0.783	0.581

Note: Chl= chlorophyll-a, B1= Band1 etc., R^2 = the coefficient of determination, RMSE = root mean square error, *=1.0e+003

Multivariate regression algorithms for turbidity (Turb) showed differences in either variable selection or statistical quality. Therefore, using the digital number values of AVHRR 5 bands for April 18, 2000, for example, according to Eq. (4.13), *Turb* can be derived by

$$Turb = -71.7451+0.0758(B1)-0.0210(B2)-0.0373(B3) +0.1208(B4)-0.0576(B5) \quad (5.15)$$

with the coefficient of determination R^2 = 0.778 and with RMSE = 1.387 FNU.

The summary of multivariate turbidity algorithms from AVHRR bands is presented in Table 5.17. The results indicate that the estimated accuracy of using multivariate turbidity algorithms is much better than that of using simple regression analyses. This means that the variation in turbidity is significantly correlated to all AVHRR bands in the study materials.

Table 5.17: The summary of turbidity retrievals from AVHRR bands.

Turb	*B1*	*B2*	*B3*	*B4*	*B5*	A_0	R^2	*RMSE*
Apr18	0.0758	-0.0210	-0.0373	0.1208	-0.0576	-71.7451	0.778	1.387
Apr21	-0.0263	0.0877	-0.0293	0.1150	-0.0079	-212.983	0.851	0.798
May02	0.1183	-0.0673	-0.0822	0.6345	0.7734	-363.719	0.944	0.524
May16	-0.0819	0.0768	0.0692	0.2102	0.0240	-82.8665	0.637	0.511

Note: Turb= turbidity, B1= Band1 etc., R^2 = the coefficient of determination, RMSE = root mean square error.

Water surface temperature (WST) was estimated using various independent variables in multivariate algorithms in this study. Using digital number values of AVHRR bands for April 18, 2000, for example, WST can be derived applying equations (4.13)

$$WST = 35.4104+0.0062(B1)-0.0009(B2)-0.0032(B3) +0.0724(B4)-0.0815(B5) \quad (5.16)$$

with the coefficient of determination R^2 = 0.559 and with the RMSE = 0.257 ^{0} C.

The summary of multivariate WST algorithms from AVHRR bands is presented in Table 5.18.

Table 5.18: The summary of WST retrievals from AVHRR bands.

WST	*B1*	*B2*	*B3*	*B4*	*B5*	A_0	R^2	*RMSE*
Apr18	0.0062	-0.0009	-0.0032	0.0724	-0.0815	35.4104	0.559	0.257
Apr21	0.0018	-0.0199	0.0078	0.0610	-0.0330	-96.3723	0.823	0.189
May02	0.0301	-0.0187	0.0055	0.8443	-0.4273	-112.933	0.861	0.260
May16	-0.0521	0.0484	0.0922	-0.3962	0.5923	-74.3391	0.817	0.222
May22	-0.0089	0.0087	0.0024	0.0278	0.0075	-98.2225	0.738	0.361
May30	-0.0267	0.0336	-0.0044	0.1150	-0.0938	-40.6105	0.975	0.187

Note: WST= water surface temperature, B1= Band1 etc., R^2 = the coefficient of determination, RMSE = root mean square error.

These results indicate that multivariate WST algorithms using AVHRR bands can provide greater ability for estimating WST variations than those using simple regression analyses.

Although the correlation coefficients between SWT and Band1, Band2 and Band3 of AVHRR are close to zero (see Table 5.18), the results using Equation (5.14) improved the SWT estimated accuracy slightly higher than that of employing the coefficients of Band1, Band2, and Band3 as zero in the study. The results also demonstrate that the retrievals of major water quality variables using multivariate empirical algorithms are better than those using simple regression analyses. This suggests that multispectral data includes more information of water characteristics. Therefore, the multivariate regression algorithms are recommended to use for surface water quality monitoring in the study area.

5.6.3 Neural network algorithms using AVHRR data

Similar empirical neural network algorithms as those employed for Landsat TM and SAR data were applied for AVHRR data. The input, on one hand, for chlorophyll-a and turbidity is AVHRR Band1 and Band2, while the input, on the other hand, for water surface temperature is AVHRR Band3, Band4 and Band5. In the hidden layer, 5 nodes were also employed to train for the output of surface water quality parameters, including chlorophyll-a (Chl-a), turbidity (Turb), and water surface temperature (WST). Table 5.19 gives the statistics for the comparison between the results using the neural network and using simple regression and multivariate regression analyses. R^2 and *RMSE* for the neural network were calculated in the same way as in the case of regression analysis.

Table 5.19: Correlation (R^2) comparison of simple regression analysis (SRA), multiple regression analysis (MRA) and neural network estimation (NNE).

	SRA			*MRA*			*NNE*		
	CHL	Turb	WST	CHL	Turb	WST	CHL	Turb	WST
Apr18	0.237	0.295	0.545	0.624	0.778	0.559	0.977	0.980	0.943
Apr21	0.115	0.595	0.531	0.407	0.851	0.823	0.776	0.809	0.801
May02	0.720	0.702	0.563	0.885	0.944	0.861	0.943	0.992	0.926
May16	0.310	0.041	0.516	0.808	0.637	0.817	0.991	0.986	0.901
May22	0.277	NA	0.707	0.543	NA	0.738	0.866	NA	0.890
May30	0.388	NA	0.733	0.738	NA	0.975	0.979	NA	0.973

Note: NA = no turbidity available

Figure 5.11 shows an example of turbidity for R^2 and *RMSE* values of the validation data set as a function of the number of hidden layer neurons on May 02, 2000. It is clear that the estimation accuracy increases with the increasing number of hidden nodes from 2 to 10. Based on experimentation, 5 hidden nodes for each input are good enough in this case study (see Fig. 5.11).

The graphical comparisons between the results of regression analysis and the neural network are shown in Figure 5.12, Figure 5.13, and Figure 5.14 as examples respectively for chlorophyll-a, turbidity, and water surface temperatures. These results clearly indicate that the performance of the neural network is much better than the performance of the regression algorithm. This is expected because of the non-linear nature of the transfer function between the surface water characteristics and satellite remote sensing observations.

These results of this study using AVHRR also support those from previous results (Zhang *et al.* 2000, Koponen 2001). Turbidity has a higher correlation with chlorophyll-a in May than in April 2000 (see Table 5.13). The probable reason is that the phytoplankton growth in the Gulf and coastal archipelago of Finland was faster in May than in April 2000. Moreover, lower correlations (R^2 = 0.043 and R^2 = 0.008) between chlorophyll-a and turbidity in April 2000 might suggest that the limiting factor at that period was the availability of both nutrients and light in the study area.

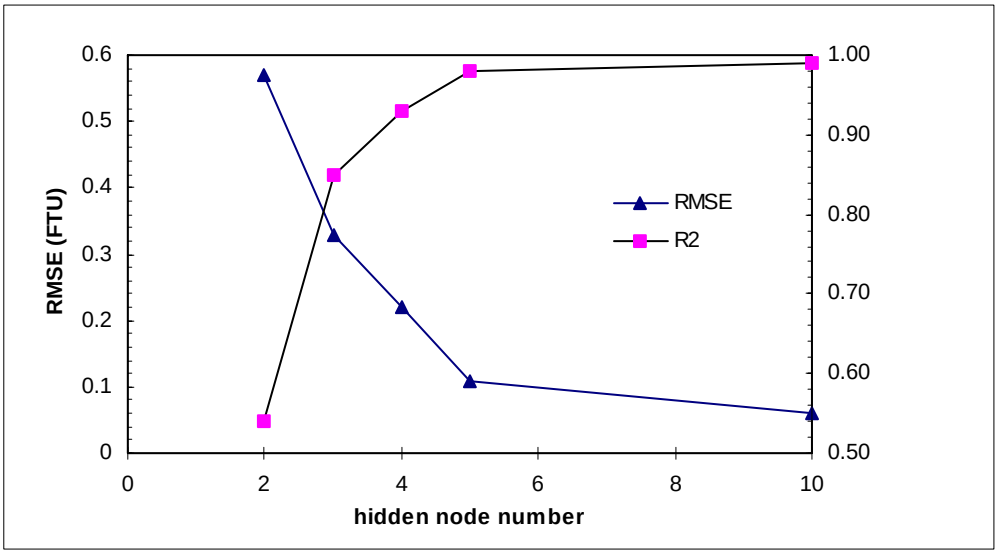

Figure 5.11 An example for R^2 and *RMSE* values of the turbidity validation data set as a function of the number of hidden layer neurons on 2nd May 2000.

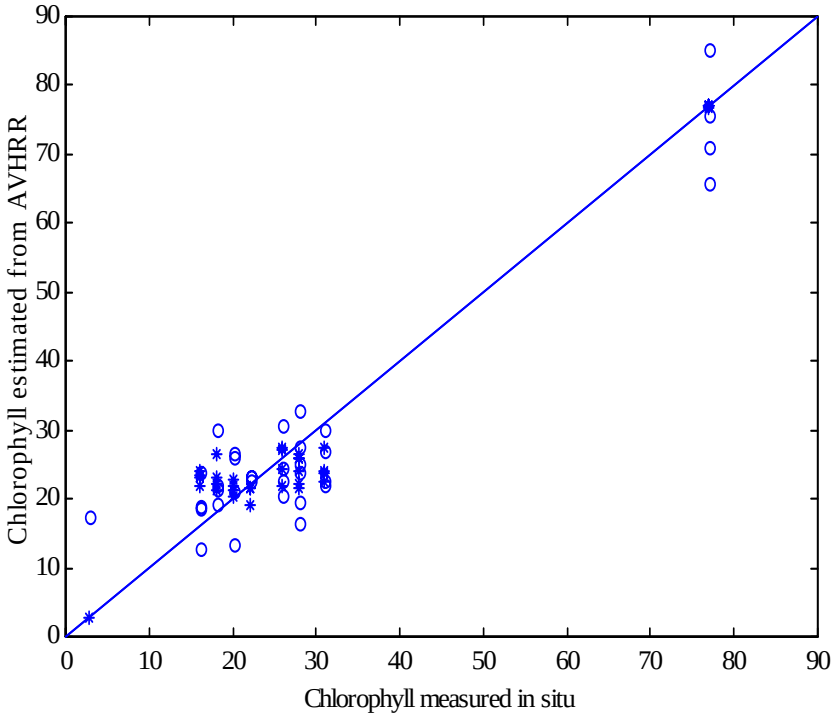

Figure 5.12: An example of the comparison between the results of regression analysis and the neural network for chlorophyll (μg /l) on 2nd May 2000.

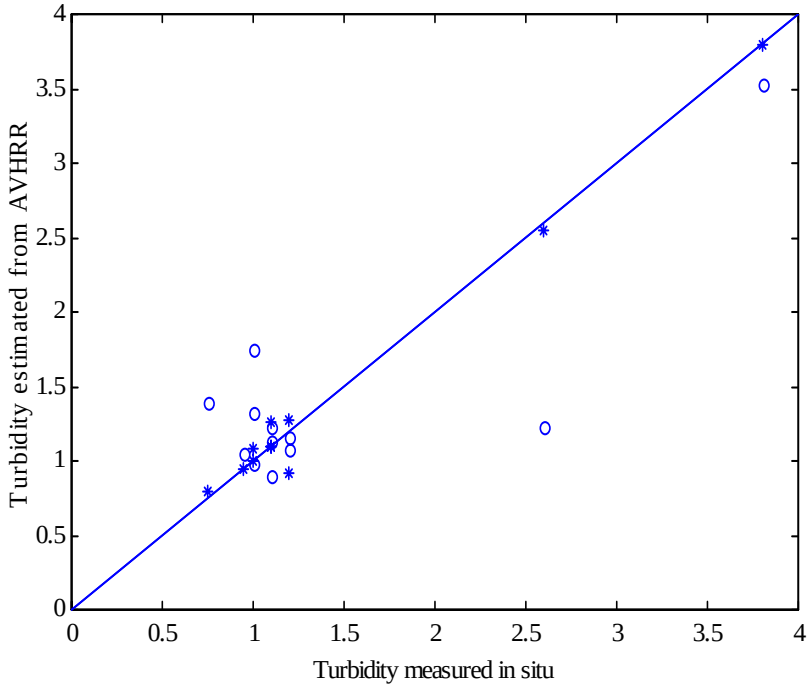

Figure 5.13: An example of the comparison between the results of regression analysis and the neural network for turbidity (FNU) on 16th May 2000.

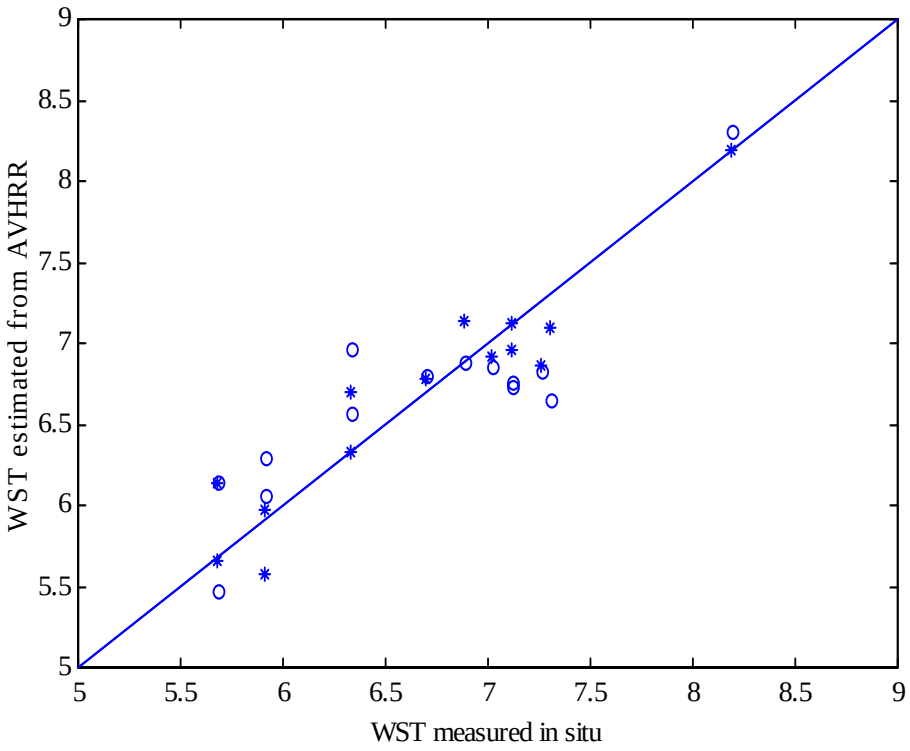

Figure 5.14: An example of the comparison between the results of regression analysis and the neural network for water surface temperature (WST) on 22nd May 2000.

More results will be presented using MODIS and MERIS data in the area in our near future studies.

5.7 Comparison of chlorophyll-a estimation using optosensors

Table 5.20 gives the comparison of chlorophyll-a estimation from AISA, Landsat TM, AVHRR and MODIS optosensors. The results indicate that the estimated accuracy of chlorophyll-a from narrow bandwidth data of optosensors (i.e., AISA and MODIS) is better than the accuracy from broad bandwidth data of optosensors (i.e., Landsat TM and AVHRR) using regression methods. In addition, the accuracy estimated from MODIS data using the neural network is slightly higher than the accuracy from Landsat TM and AVHRR data, even though the neural network was not yet applied to AISA data due to its large band numbers.

Table 5.20: Comparison of estimated results from AISA, Landsat TM, AVHRR and MODIS sensors.

R^2	AISA	LandsatTM	AVHRR	MODIS
Regression	0.872	0.655	0.530	0.761
NeuralNet	Not yet	0.903	0.979	0.987

These and the previous results (e.g., Pullianen *et al.* 2001, Koponen *et al.* 2001 and 2002) also show that the spectral resolution of remote optosensors is more significant than the spatial resolution of optosensors for water quality studies in the study region [P2].

5.8 Discussion

In the international literature, water quality studies have shown results similar with those in this thesis. The results for individual scenes are not very consistent and show variability from 0.59 to 0.98 in R^2 (Lindell *et al.* 1999). For example, Dekker and Peters (1993) retrieved Secchi disk death (SDD) with $R^2 = 0.66$ using Landsat TM data for their Dutch lakes. Lathrop *et al.* (1991) applied Landsat TM data to estimate turbidity for Green Bay and Central Lake Michigan with $R^2 = 0.84$. Lavery *et al.* (1993) got $R^2 = 0.81$ of the SDD retrieval for the Western Australia coast. Tassan (1987) estimated total suspended sediment (TSS) from TM data with $R^2 = 0.92$. Lindel *et al.* (1999) produced a $R^2 = 0.86$ of chlorophyll-a estimation in Sweden lakes. Since values of water quality variables in the lakes and coastal areas of these countries were different from those in Finland, the results in this study are not same as theirs. For example, Koponen *et al.* (2002) derived SDD, turbidity, and chlorophyll-a for Finnish Lakes with $R^2 = 0.92$, $R^2 = 0.85$, and $R^2 = 0.93$, respectively. In this thesis, however, the best results of SDD, turbidity, and chlorophyll-a are $R^2 = 0.95$, $R^2 = 0.96$, and $R^2 = 0.92$, respectively. These previous results show that water quality variables can be estimated using remotely sensed data with reasonable accuracy, but the limitation is their specific algorithms in different areas.

6. CONCLUSIONS

In this study, remote sensing of water as well as basic radiative transfer theory and simulation methods on optical properties of natural waters were first reviewed. Semi-empirical, simple regression and multivariate regression analysis, and neural network algorithms of surface water quality estimation were then applied using optical (e.g., AISA, Landsat TM, AVHRR and MODIS) data and microwave (e.g., ERS-2 SAR) data for the Gulf of Finland and the Finnish Archipelago Sea in August 1997 and from April to May 2000, respectively.

The focus in this study was on the following subjects:

- Up to date, the digital evaluation of remotely sensed data has been used to estimate water quality parameters in lakes and coastal areas. Most of retrievals are employed empirical algorithms. They can provide site-specific predictions of water quality parameters with a reasonable accuracy, but are limited in their universal application. It is necessary to develop standard algorithms for a comprehensive analysis of surface water quality estimation in the Gulf of Finland and the Finnish Archipelago Sea.
- The result of SDD using the semi-empirical algorithm is not very good, obviously because the assumptions were adopted when the algorithm was deduced. For example, the retrieved R^2 for SDD is 0.521, which is smaller than that of SDD using the single red band (TM3) (R^2 = 0.530) in the simple regression analysis. This means that single band or band ratio algorithms can be used to estimate SDD instead of the semi-empirical ones in the area.
- Simple regression analysis was applied to find the relationship between single bands (or band ratios and their combinations) and water quality parameters in the area. The highest relation (R^2 = 0.664) is that of the red band (TM3) and turbidity. It has also demonstrated that band ratios (e.g., blue-to-green ratios) do not provide the best result for chlorophyll-a retrieval in the area. However, their combinations show better results than single bands or band ratios, e.g., for chlorophyll-a with (R^2 = 0.677), for suspended sediment with (R^2 = 0.542), for turbidity with (R^2 = 0.690), and for SDD with (R^2 = 0.724).
- Multivariate regression analysis was used to estimate water quality parameters resulting in higher accuracy than those of using semi-empirical algorithm and

simple regression analysis. This is because multi-spectral TM bands can provide more information of surface water conditions than single bands or band ratios, for example, chlorophyll-a as (R^2 = 0.542), suspended sediment as (R^2 = 0.572), turbidity as (R^2 = 0.709), and SDD as (R^2 = 0.740). However, the chlorophyll-a retrieval (R^2 = 0.542) of using multivariate egression is not as good as that of using their combinations of single bands and band ratios (R^2 = 0.677). In addition, band ratios and their combinations of narrow bands (e.g., AISA and MODIS) have a better ability than those of broad bands (e.g., TM and AVHRR) to retrieve chlorophyll-a, e.g., for band ratios of AISA data as (R^2 = 0.872) and for their combination of MODIS data as (R^2 = 0.761). Therefore, a comprehensive analysis of the performance of standard algorithms should be beneficial for the current use of remote sensing data and future efforts on algorithm development.

- The results indicated that the neural network adequately described the non-linear transfer function between the Landsat TM and ERS-2 SAR observations and the major water quality variables of surface waters, e.g., chlorophyll-a with (R^2 = 0.903), suspended sediment with (R^2 = 0.888), turbidity with (R^2 = 0.942), and SDD as (R^2 = 0.916). Clearly, these results are much better than those of using semi-empirical algorithm, simple and multivariate regression analyses. This is because the neural network is able to model the non-linear transfer function with a higher accuracy than the algorithms of traditional regression analyses.
- The additional use of SAR data combined with TM data in multivariate regression analysis and neural network algorithms can slightly improve the approximation for parameters in surface waters at about 3.5%. However, this small improvement is only marginal to estimate water quality parameters in our case study.
- AVHRR can be applied to monitor surface water conditions, e.g., chlorophyll-a and/or turbidity and water surface temperature in the area. But AVHRR data are not sensitive to chlorophyll-a changes in our case study.

7. FUTURE RESEARCH

Remote sensing of water quality in the Gulf of Finland will be further investigated. Future studies will be focused on the following:

1) AISA spectrometer data (430-900 nm) will be further used to develop empirical algorithms which can also be applied to more MODIS and new MERIS data in the Gulf of Finland;
2) Thermal infrared (TIR) data and microwave data from new sensors onboard the ESA ENVISAT-1 satellite (e.g., MERIS and ASAR data) will be further applied to water quality studies in the study area;
3) Semi-empirical algorithms for surface water quality variables such as Secchi disk depth, turbidity and chlorophyll-a will be developed using new satellite optical data;
4) Sea surface temperature (SST) and other factors affecting surface water quality retrievals will be further evaluated in future studies.

8. SUMMARY OF THE APPENDED PAPERS

[P1]

Empirical algorithms for determining the Secchi disk depth (SDD) are developed and employed using optical (e.g., Landsat TM) and microwave (e.g., ERS-2 SAR) remotely sensed data from the Gulf of Finland and the Archipelago Sea. The SDD is an important optical measure of water quality in the study area, where the coastal water considerably attenuates light because of the presence of phytoplankton, suspended matter and yellow substance. A semi-empirical algorithm of SDD was developed in this study, by which the result of using the semi-empirical algorithm was also compared with results of using multivariate regression and neural network methods. The obtained results show that the accuracy of SDD estimation using a neural network-based method is much higher that of the semi-empirical or multivariate approach. On the other hand, the additional use of SAR data only slightly improved SDD estimation when compared with the use of TM data only. Although the improvement is marginal, the results suggest that there may be some SAR backscattering signatures correlated to SDD measurements in the area. However, such a small improvement is not very helpful for the practical estimation of SDD. In the future, the technique of using combined optical and microwave data still needs to be refined using, e.g., MERIS and ASAR data.

[P2]

Chlorophyll-a is one major factor affecting water environment and produces visible changes in the surface of water. Such changes in the water surface are measurable with remote optosensors. This paper describes an application of neural networks to chlorophyll-a estimation in coastal waters in the Gulf of Finland using remote optosensors. AISA data was employed to develop empirical algorithms in this study, while Landsat TM, AVHRR and MODIS data were applied to estimate chlorophyll-a. The comparison of chlorophyll-a estimation from AISA, TM, AVHRR and MODIS optosensors was presented in the study. The results indicated that the estimated accuracy of chlorophyll-a from narrow bandwidth data of optosensors (i.e., AISA and MODIS) is better than the accuracy from broad bandwidth data of optosensors (i.e.,

TM and AVHRR) using regression methods. In addition, the accuracy estimated from MODIS data using the neural network is slightly higher than the accuracy from TM and AVHRR data, even though the neural network was not applied to AISA data due to its large band numbers. The results also show that the spectral resolution of remote optosensors is more significant than the spatial resolution of optosensors for water quality studies in the region.

[P3]

Observations of turbidity, Secchi disk depth, and suspended sediment concentration provide quantitative information concerning water quality conditions. Additionally, these observations can be used in various numerical schemes to help characterize the trophic state of an aquatic ecosystem. Currently, the digital evaluation of Landsat TM information at visible and near infrared (NIR) wavelengths has been used to estimate water quality variables. Although Landsat TM sensor is able to present a synoptic monitoring of water quality problems, its quantitative use is a difficult task.

On the other hand, radar remote sensing is quite different from optical remote sensing in many ways. A radar signal does not significantly penetrate into the water. Instead, it reflects from the water surface. Hence, the radar backscattering signatures can only carry information on: 1) water surface geometry (waves and ripples); 2) materials on water surface; and 3) permittivity (dielectric constant) of water top layer. Nevertheless, water surface geometry can be related to such properties as water bottom topography, internal waves/currents, and slicks on surface. The obtained results indicate that the network is able to model the nonlinear transfer function with higher accuracy than algorithms based on traditional regression analyses, although the regression analyses are still good methods to apply for transfer functions in which linear behaviour or nonlinear transfer functions are well known. In addition, both multivariate and neural network approaches using combined TM and SAR data improves very little (e.g., less than 5%) the estimation accuracy of these water quality variables.

[P4]

Four major parameters of surface water quality such as chlorophyll-a, suspended sediment concentration, turbidity and Secchi disk depth were estimated using an empirical neural network algorithm from the combined optical (i.e., Landsat TM) data and microwave (i.e., ERS-2 SAR) data in the Gulf of Finland. The results of using the empirical neural network were compared with those of using traditional regression analyses. Application of this neural network shows that the estimation accuracy for these major characteristics of surface waters is much better than those from regression analyses. The results also indicate that microwave data can assist to improve the estimation of these characteristics, although the improvement obtained for parameter retrieval is limited in the study area. This means that it is possible to develop surface water quality algorithms in which microwave data are used as supplementary data to optical observations.

In addition, thermal data (TM6) from Landsat TM was also taken into account in this study, although TM6 is measuring the emitted thermal radiance of the water body and not the reflected light. It is true that the thermal data (TM6) has no or very little effects on optical measurements such as SDD as they are relatively weakly correlated to the sea surface properties. Since water surface temperature is mainly related to the emission properties and the physical temperature of water body, the surface roughness has an effect on thermal radiance. The results in the study demonstrate that the TM6 does have some effects on Chl-a, SSC and turbidity retrievals, but it has almost no improvement to SDD. Therefore, the relationship between water surface temperature and surface water quality still needs to be further investigated in future studies.

[P5]

Optical, thermal infrared (TIR), and microwave remotely sensed data were separately applied to chlorophyll-a and turbidity estimation in the study. Although the previous studies were also dealing with water quality retrievals in coastal waters of the Gulf of Finland using combined optical and microwave data, the contribution of TIR data to chlorophyll-a and turbidity estimation was not separately discussed before.

TIR and microwave remote sensing are significantly related to the surface roughness of water. Both TIR and microwave sensors measure water surface

properties, instead of the water mass below the surface. This means that the TIR sensor measures the emitted thermal radiance of the water body, but not the reflected radiance from the water surface. Since the water surface temperature is mainly related to the emission properties and the physical temperature of water body, the surface roughness has an effect on thermal radiance. The results indicate that the contribution of TIR to chlorophyll-a and turbidity estimation is up to 9.9% and 1.5% using multivariate regression analysis, while microwave data only improved 1.9% and 0%, respectively. On the other hand, improvements of chlorophyll-a (6.2%) and turbidity (6.7%) from TIR data using the neural network are slightly better than those of 3% and 3.5% from microwave data, respectively. The reason for such different improvements still needs further investigations.

[P6]

Satellite remote sensing provides an adequate synoptic and repetitive overview of environmental parameters in oceanography, especially in the coastal areas where sea surface temperature (SST) monitoring allows a precise description of upwelling's dynamic. Passive infrared remote sensing such as NOAA AVHRR is one of the techniques used for Earth surface observations from space.

SST measurement using AVHRR thermal infrared (TIR) band data is now an operation reality. However, the error factors in the SST estimation are not limited to the atmospheric effects. Sea surface effects (SSE) were surveyed to suggest that it should be a mainly error factor. The SSE includes salinity of sea water and wind speed, affecting the emission of the sea surface. The results show that there is a difference between SST and the water temperature below the sea surface. Such a difference is mainly affected by the salinity and wind speed, which will be further discussed in future studies.

9. REFERENCES

Aiken, J., Moore, G.F., Trees, C.C., Hooker, S.B. and D.K. Clark (1995), The SeaWiFS CZCS type pigment algorithms. SeaWiFS Technical Rep. Series, NASA Techn. Memo. 104566, Greenbelt, Maryland, 34 p.

Alföldi, T., and Munday, J. C. (1978), Water quality analysis by digital chromaticity mapping of Landsat data. *Canadian J. Remote Sens.* 4:108-122.

Alpers, W., Ross, D. B. and Rufenach, C. L. (1981), On the detectability of ocean surface waves by real and synthetic aperture radar. *J. Geophys. Res.* 86:6481-6498.

Arst, H. and Kutser, T. (1994), Data-processing and interpretation of sea radiance factor measurements. *Polar Research,* 13: 3-12.

Arst, H., Maekivi, S., Lukk, T., and Herlevi A. (1997), Calculating irradiance penetration into water bodies from the measured beam attenuation coefficient. *Limnol. Oceanogr.*, 42: 379-385.

Astok, V., Hannus, M., Jaanus, A. (1991), The state of the coastal waters of the eastern part of the Gulf of Finland in the 1980's. General conclusions. *Baltic Sea Environ. Proceedings,* 40: 70-74.

Austin, R. W., and Petzold, T. J. (1981), Water colour measurements. In Gower, J. F. R. (ed.), *Oceanogr. from Space*, Plenum, New York, pp. 239-256.

Baban, S. M. J. (1993), Detecting and evaluating the influence of water depth, volume and altitude on the variations in the surface temperature of lakes using Landsat imagery. *Int. J. Remote Sens.*, 14: 2747-2758.

Beal, R. C., Tilley, D. G. and Monaldo, F. M. (1983), Large and small scale spatial evolution of digitally processed ocean wave height spectra from SEASAT synthetic aperture radar. *J. Geophys. Res.*, 88: 1761-1778.

Beale, R., and Jackson, T. (1990), *Neural Computing: An introduction,* Adam Hilger, Bristol, UK.

Benediktsson, J. A., and Kanellopoulos, I. (1999), Information extraction based on ultisensor data fusion and neural networks. In Chen, C. H. (ed.), *Information Processing for Remote Sensing*, pp. 369-395.

Braga, C. Z. F., Setzer, A. W., and de Lacerda, L. D. (1993), Water quality assessment with simultaneous Landsat-5 TM data at Guanabara Bay, Rio de Janeiro, Brazil. *Remote Sens. Environ.* 45: 95-106.

Broschat, S. L. (1993), The small slope approximation reflection coefficient for scattering from a "Pierson-Moskowitz" sea surface. *IEEE Trans. Geosci. Remote Sens.,* 31: 1112-1114.

Bruning, C., Alpers, W., Zambresky, L. F. and Tilley, D. G. (1988), Validation of a synthetic aperture radar ocean wave imaging theory by the Shuttle Imaging Radar-B experiment over the North Sea. *J. Geophys. Res.,* 93: 15,403-15,425.

Bukata, R. P., Jerome, J. H., Kondratyev, K. Y. A. and Pozdnyakov, D.V. (1991), Satellite monitoring of optically-active components of inland waters: an essential input to regional climate change impact studies. *J. Great Lakes Res.,* 17(4): 470-478.

Bukata, R. P., Jerome, J. H., Kondratyev, K. Y. A., and Pozdnyakov, D. V. (1995), *Optical Properties and Remote Sensing of Inland and Coastal Waters,* (Boca Raton, Florida: CRC Press Inc.), 362 p.

Cairns, S.H., Dickson, K.L, and Atkinson, S.F. (1997), An examination of measuring selected water quality trophic indicators with SPOT satellite HRV data, *Photogramm. Eng. Remote Sens.,* 63: 263-265.

Campbell, J.W., Blaisdell, J.M., and Darzi, M. (1995), Levael-3 SeaWiFS data products: spatial and temporal binning algorithms. SeaWiFS Technical Rep. Series, NASA Techn. Memo. 104566, Greenbelt, Maryland, 76 p.

Chavez, P.S. Jr. (1988), An improved dark-object subtraction technique for atmospheric scattering correction of multispectral data. *Remote Sens. Environ.,* 24: 459-479.

Chavez, P.S. Jr. (1996), Image-based atmospheric corrections-revised and improved. *Photogramm. Eng. Remote Sens.* 62: 1025-1036.

Chen, K.S., Fung, A.K. and Weissmann, D.E. (1992), A backscattering model for ocean surface. *IEEE Trans. Geosci. Remote Sens.,* 30: 811-817.

Cracknell, A.P. (1997), *The Advanced Very High Resolution Radiometer,* (Taylor & Francis Ltd, Gunpowder Square, London EC4A 3DE), 534 p.

Curran, P.J., and Novo, E.M.M. (1988), The relationship between suspended sediment concentration and remotely sensed spectral radiance: a review. *J. Coastal Research.* 4: 351-368.

D'Alimonte, D., Melin, F., and Zibordi, G., and Berthon, J.F. (2003), Use of the novelty detection technique to identify the range of applicability of empirical ocean color algorithms. *IEEE Trans.Geosci. Remote Sens.,* 41: 2833-2843.

Darecki, M. and Stramski, D. (2004), An evaluation of MODIS and SesWiFS bio-optical algorithms in the Baltic Sea. *Remote Sens. Environ.,* 89: 326-350.

Darecki, M., Weeks, A., Sagan, S., Kowalczuk, P. and Kaczmarek, S. (2003), Optical characteristics of two contrasting Case 2 waters and their influence on remote sensing algorithms. *Continental Shelf Res.,* 23: 237-250.

Dekker, A.G., and Peters, S.W.M. (1993), The use of the Thematic Mapper for the analysis of eutrophic lakes: a case study in the Netherlands. *Int. J. Remote Sens.,* 14: 799-821.

Doerffer, R., Fischer, J., Stossel, M., and Brockmann, C. (1989), Analysis of Thematic Mapper data for studying the suspended matter distribution in the coastal area of the Germany Bight (North Sea). *Remote Sens. Environ.* 28: 61-73.

Dwivedi, R. M., and Narain, A. (1987), Remote sensing of phytoplankton: an attempt from the Landsat Thematic Mapper. *Int. J. Remote Sens.* 8: 1563-1569.

Eloheimo, K., Hannonen, T., Härmä, P., Kutser, T., Pyhälahti, T., Vepsäläinen, J., Sucksdorff, Y., Vuorimies, J., Pulliainen, J., Koponen, S., Servomaa, H., Tauriainen, S., and Zhang, Y. (1997), *Operative Monitoring System for Coastal Waters of the Baltic Sea* (draft report for TEKES).

Eloheimo, K., Hannonen, T., Härmä, P., Pyhälahti, T., Koponen, S., Pulliainen, J., Servomaa, H. (1998), Coastal monitoring using satellite, airborne and *in situ* data in the archipelago of Baltic Sea. *Proc. 5th Int. Conference Remote Sens. Marine and Coastal Environ.*, 5-7 Oct., San Diego, CA.

Erkkila, A. and Kalliola, R. (2004), Patterna and dynamics of coastal waters in multi-temporal satellite images: support to water quality monitoring in the Archipelago Sea, Finland. *Estuarine Coastal and Shelf Science,* 60: 165-177.

Gilabert, M.A., Conese, C., and Maselli, F. (1994), An atmospheric correction method for the automatic retrieval of surface reflectances from TM images. *Int. J. Remote Sens.*, 15: 2065-2086.

Gordon, H. R. and Clark D.K. (1980), Atmospheric effects in the remote sensing of phytoplankton pigments. *Boudary-layer Meteorol.,* 18: 299-313.

Gordon, H. R., Clark, D. K., Brown, J. W., Brown, O. B., Evans, R. H. and Broenkow, W. W. (1983), Phytoplankton pigment concentrations in the Middle Atlantic Bight: comparison of ship determinations and CZCS estimates. *Appl. Opt.*, 22: 20-36.

Gordon, H. R., and Morel, A.Y. (1983), *Remote Assessment of Ocean Color for Interpretation of Satellite Imagery - A Review,* Spring-Verlag, New York.

Gordon, H. R., Brown, O. B., Evans, R. H., Brown, J. W., Smith, R.C., Baker, K.S. and Clark, D. K. (1988), A semianalytical radiance model of ocean color. *J. Geophys. Res.,* 93(D9): 10,909-10,924.

Gould, R.W., Jr., and Arnone, R.W. (1997), Estimating the beam attenuation coefficient in coastal waters from AVHRR imagery. *Remote Sens. Environ.* 63: 701-705.

Hallikainen, M. (1999a), Development of sensors and methods for remote sensing of Northern areas by HUT laboratory of space technology. *IEEE Geosci. Remote Sens. Newsletter, Dec., ISSN 0161-7869,* 107: 10-11.

Hallikainen, M. (1999b), *Annual Report 1998,* Laboratory of Space Technology at HUT, Espoo, Report 36: 36-39.

Hasselmaan, K., Raney, R. K., Plant, W. J., Alpers, W., Shuchman, R. A., Lyzenga, D. R., Rufenach, C. L. and Tucker, M. J. (1985), Theory of SAR ocean wave imaging, a MARSEN view. *J. Geophys. Res.,* 90: 4659-4686.

Herlevi, A. (2002), *Inherent and Apparent Optical Properties in Relation to Water Quality in Nordic Waters,* Doctoral Thesis, University of Helsinki, No. 45, 57 p.

Hu, C., Carder, K.L., and Muller-Karger, F.E., (2000), How precise are SeaWiFS ocean color estimates? Implications of digitization-noise errors. *Remote Sens. Environ.* 76: 239-249.

Ishimaru, A. (1978), *Wave Propagation and Scattering in Random Media,* Academic Press, New York, 572 p.

Jerlov, N. G. (1976), *Marine Optics, Elsevier Oceangraphy Series 14,* Elsevier Publishing Co., Amsterdam, 231 p.

Kauppila, P., Hällfors, G., Kangas, P., Kokkonen, P., Basova, S. (1995), Late summer phytoplankton species composition and biomasses in the eastern Gulf of Finland. *Ophelia.* 42: 179-191.

Keiner, L. E., and Yan, X. (1998), A neural network model for estimating sea surface chlorophyll and sediments from Thematic Mapper Imagery. *Remote Sens. Environ.* 66: 153-165.

Keiner, L. E. (1999), Neural networks as non-linear function approximation for remote sensing applications. In Chen, C. H., editor, *Information Processing for Remote Sensing,* World Scientific Publishing Co., Singapore, pp. 213-223.

Khorram, S., and Cheshire, H.M. (1985), Remote sensing of water quality in the Neuse river estuary, North Carolina. *Photogramm. Eng. Remote Sens.* 51: 329-341.

Klemas, V., Bartlett, D., Philpot, W., and Roger, R. (1974), Coastal and estuarine studies with ERTS-1 and Skylab. *Remote Sens. Environ.*, 3: 153-177.

Kononen, K. (1992), Dynamic of the toxic cyanibacterial blooms in the Baltic Sea. *Finnish Marine Research.*, 261: 3-36.

Koponen, S. (2001), *Remote Sensing of Water Quality for Finnish Lakes,* Licentiate Thesis, Laboratory of Space Technology, Helsinki University of Technology, Finland, 45 p.

Koponen, S., Pulliainen, J., Servomaa, H., Zhang, Y., Hallikainen, M., Kallio, K., Vepsäläinen, J., Pyhälahti, T., and Hannonen, T. (2001), Ananlysis on the feasibility of multisource remote sensing observations for chl-a monitoring in Finnish lakes. *The Science of the Total Environment,* 268: 95-106.

Koponen, S., Pulliainen, J., Kallio, K., and Hallikainen, M. (2002), Lake water quality classification with airborne hyperspectral spectrometer and simulated MERIS data. *Remote Sens. Environ.*, 79: 51-59.

Kowalczuk, P. (1999), Seasonal variability of yellow substance absorption in the surface layer of the Baltci Sea. *J. Geophys. Res.* 104: 30,047-30,058.

Krasnopolsky, V., Breaker, L., and Gemmill, W. (1995), A neural network as a nonlinear transfer model for retrievling surface wind speeds from the special sensor microwave imager. *J. Geophys. Res.* 100 (C6): 11,033-11,045.

Krasnopolsky, V., Gemmill, W., and Breaker, L. (2000), A neural network multi-parameter algorithm for SSM/I ocean retrievals: comparisons and validations. *Remote Sens. Environ.* 73: 133-142.

Kratzer, S., Hakansson, B., and Sahlin, C. (2003), Assessing Secchi and photic zone depth in the Baltic Sea from satellite data. *AMBIO,* 32: 577-585.

Kutser, T., (1997), *Estination of Water Quality in Turbid Inland and Coastal Waters by Passive Optical Remote Sensing,* Doctor thesis, University of Tartu, Estonia.

Kuusisto., M., Koponen, J., and Sarkkula, J. (1998), Modelled phytoplankton dynamics in the Gulf of Finland. *Enviorn. Modelling and Software.* 13: 461-470.

Lahet, F., Ouillon, S., and Forget, P. (2000), A three-component model of ocean color and its application in the Ebro river mouth area. *Remote Sens. Environ.* 72: 181-190.

Lathrop, R.G., Jr., and Lillesand, T.M. (1986), Use of Thematic Mapper data to assess water quality in Green Bay and central Lake Michigan. *Photogramm. Eng. Remote Sens.*, 52: 671-680.

Lathrop, R. G., Lillesand, T. M., and Yandell, B. S. (1991), Testing the utility simple multi-date Thematic Mapper calibration algorithms for monitoring turbid inland waters. *Int. J. Remote Sens.* 12: 2045-2063.

Lavery, P., Pattiaratchi, C., Wyllie, A., and Hick, P. (1993), Water quality monitoring

in estuarine water using the Landsat Thematic Mapper. *Remote Sens. Environ.* 46: 268-280.

Leivuori, M. Vallius, H. (1998), A Case study of seasonal variation in the chemical compsition of accumulating suspended sediments in the central Gulf of Finland. *Chemosphere,* 36: 503-521.

Lillesand, T.M., Johnson, W.L., Deuell, R.L., Lindstrom, O.M. and Miesner, D.E. (1983), Use of Landsat data to predict trophic status of Minnesota lakes. *Photogramm. Eng. Remote Sens.* 49: 219-229.

Lindell, L.T., Jonsson, O.S.M., and Claesson, TH. (1985), Mapping of coastal water turbidity using Landsat imagery. *Int. J. Remote Sens.,* 6: 643-656.

Lindell, T., Pierson, D., Premazzi, G., and Zilioli, E. (1999), Manual for monitoring European lakes using remote sensing techniques, (Luxembourg: Official Pulications of the European Communities), EUR 18665 EN, 161 p.

Masters, T. (1993), *Practical Neural Network Recipes in C++,* Academic, San Diego, CA.

McClain, C.R., Cleave, M.L., Feldman, G.C., Gregg, W.W., and Hooker, S.B. (1998), Science quality SeaWiFS data for global biosphere research. *Sea Tech.* 39: 10-16.

Monaldo, F.M. and Lyzenga, D.R. (1986), On the estimation of wave slope- and height- variance spectra from SAR imagery. *IEEE Trans. Geosci. Remote Sens.,* GE-24: 543-551.

Moore, G. K. (1980), Satellite remote sensing of water quality. *Hydrol. Sci.* 25: 407-421.

Morel, A., and Prieur, L. (1977), Analysis of variation in ocean color. *Limnol. Oceanogr*. 22: 709-722.

Morel, A. (1980), In-water and remote measurements of color. *Boundary-layer Meteorol.,* 18: 177-201.

Morel, A. (1988), Optical modelling of the upper ocean in relation to its biogenous matter content (case I waters). *J. Geophys. Res.,* 93: 10,749-10,768.

Morel, A. and Gentili, B. (1990), Diffuse reflecatance of oceanic waters: Its dependence on Sun angle as influenced by the molecular scattering contribution. *Appl. Opt.,* 30: 4427-4438.

Munday, J.C., and Zubkoff, P.L. (1981), Remote sensing of dinoflagellate blooms in the turbid estuary. *Photogramm. Eng. Remote Sens.* 47:523-531.

Nilsson, C.S. and Tildesley, P.C. (1995), Imaging of oceanic features by ERS-1 synthetic aperture radar. *J. Geophys. Res.,* 100: 953-967.

Nyfors, E. and Vainikainen, P. (1989), *Industrial Microwave Sensors,* Artech House, 351 p.

O'Reilly, J.E., Maritorena, S., Mitchell, B.G., Siegel, D.A., Carder, K.L., Garver, S.A., Kahru, M., and McClain, C.R. (1998), Ocean color chlorophyll algorithms for SeaWiFS. *J. Geophys. Res.* 103: 24937-24953.

Ouaidrari, H., and Vermote, E.F. (1999), Operational atmospheric correction of Landsat TM data. *Remote Sens. Environ.,* 70: 4-15.

Pattiaratchi, C., Lavery, P., Wyllie, A., and Hick, P. (1994), Estimates of water quality in coastal waters using multidate Landsat Thematic Mapper data. *Int. J. Remote Sensing,* 15: 1571-1584.

Pitkänen, H., Kangas, P., Sarkkula, J., Lepistö, L., Hällfors, G., and Kauppila, P. (1990), Water quality and trophic status in the eastern Gulf of Finland. *Publications of the Water and Environ. Admin.,* Series A 50: 1-134.

Pitkänen, H. (1991), Nutrient dynamics and trophic conditions in the eastern Gulf of Finland: the regulatory role of the Neva estuary. *Aqua Fennica.,* 21: 105-115.

Pitkänen, H., Tamminen, T., Kangas, P., Huttula, T., Kivi, K., Kuosa, H., Sarkkula, J., Eloheimo, K., Kauppila, P., and Skakalsky, B. (1993), Late summer trophic conditions in the north-east Gulf of Finland and the River Neva estuary, Baltic Sea. *Estuarine Coastal and Shelf Sci.* 37: 453-474.

Platt, T., Caverhill, C., and Sathyendranath, S. (1991), Basinscale estimates of oceanic primary production by remote sensing: the North Atlantic. *J. Geophys. Res.,* 93: 10,749-10,768.

Populus, J., Moreau, F., Coquelet, D., and Xavier, J.-P. (1995), An assessment of environmental sensitivity to marine pollutions: solutions with remote sensing and geographic information systems (GIS). *Int. J. Remote Sensing*, 16: 3-15.

Pulliainen, J., Kallio, K., Eloheimo, K., Koponen, S., Servomaa, H., Hannonen, T., Tauriainen, S., and Hallikainen, M. (2001), A semi-operational approach to water quality retrival from remote sensing data. *The Science of the Total Environment*, 268: 79-93.

Ruddick, K.G., Ovidio, F., and Rijkeboer, M. (2000), Atmospheric correction of SeaWiFS imagery for turbid coastal and inland waters. *Appl. Opt.,* 39: 897-912.

Shuchman, R.A. and Shemdin, O.H. (1981), SAR imaging of the ocean surface waves during the Marineland experiment. *IEEE J. Oceanic Eng.*, OE-8: 83-90.

Smith, R.C., and Baker, K.S. (1978), The bio-optical state of ocean waters and remote sensing. *Limnol. Oceanogr.,* 23: 247-259.

Spinrad, R. W., Glover, H., Ward, B.B., Codispoti, L.A. and Kullenberg, G. (1989), Suspended particle and bacterial maxima in Peruvian coastal water during a cold water anomaly. *Deep Sea Res.,* 36: 715.

Strong, A.E., (1974), Remote sensing of algal blooms by aircraft and satellite in Lake Erie and Utah Lake, *Remote Sens. Environ.*, 3: 99-107.

Sucksdorff, Y., Härmä, P., Jänne, S., Metsämäki, S., and Pyhälahti, T. (1997), *NOAA AVHRR Data Processing Software*, Finnish Environment Institute, Helsinki.

Särkkä, J., Järvet ja Ympäristö (1996), *Limnologian Perusteet* (In Finnish), Helsinki, Gaudeamus, 157 p.

Tamminen, T. (1990), Eutrophication and the Baltic Sea: studies on phytoplankton, bacterioplankton and pelagic nutrient cycles. PhD thesis, Department of Environmental Conservation, University of Helsinki, Finland.

Tassan, S. (1987), Evaluation of the potential of the Thematic Mapper for marine application. *Int. J. Remote Sens.*, 8: 1455-1478.

Tassan, S. (1994), Local algorithms using SeaWiFS data for the retrieval of phytoplanlton, pigments, suspended sediment, and yellow substance in coastal waters. *Appl. Opt.*, 33: 2369-2378.

Ulaby, F. T. (1981), *Microwave Remote Sensing: active and passive*, Vol. I, Addison-Wesley Publishing Company, Reading Massachusetts.

Ulaby, F. T., Moore, R. K. and Fung, A. K. (1982), Radar remote sensing and surface scattering and emission theory. *Microwave Remote Sensing: active and passive*, Vol. II, Addison-Wesley Publishing Company, Reading Massachusetts, pp. 853-860.

Vermote, E.F., Tanre, D., Deuze, J.L., Herman, M., and Morcrette, J.J. (1995), A 6S user guide version 1. *Universite des Sciences et Tecnologies de Lille*, Lille.

Vermote, E.F., Tanre, D., Deuze, J.L., Herman, M., and Morcrette, J.J. (1997), Second simulation of the satellite signal in the solar spectrum, 6S: an overview. *IEEE Trans. Geosci. Remote Sens.*, 35: 675-686.

Vesecky, J.F. and Stewart, R.H. (1982), The observation of ocean surface phenomena using imagery from SAESAT synthetic aperture radar: An assessment. *J. Geophys. Res.*, 87: 3397-3430.

Vogelzang, J., Wensink, G.J., van der Kooij, M.W.A. and van Swol, R. (1994), Mapping of sea bottom topography with ERS-1 C-band SAR, Proceedings of Second ERS-1 Symposium, Space at the service of our environment. *Eur. Space Agency Spec. Publ. ESA SP-361(2),* pp. 945-948.

Vogelzang, J. (1997), Mapping submarine sand waves with multiband imaging radar, 1. Model development and sensitivity and analysis. *J. Geophys. Res.*, 102:1163-1181.

Whitlock, C. H., Poole, L. R., Usry, J. W., *et al.* (1981), Comparison of reflectance with backscatter and absorption parameters for turbid waters. *Appl. Opt.,* 20: 517-522.

Woodruff, D. L., Stumpf, R. P., Scope, J. A. and Paerl, H. W. (1999), Remote estimation of water clarity in optically complex estuarine waters. *Remote Sens. Environ.,* 68: 41-52.

Zhang, M., Carder, K., Muller-Karger, F.E., Lee, Z. and Gold, D.B. (1999), Noise reduction and atmospheric correction for coastal applications of Landsat Themtic Mapper. *Remote Sens. Environ.* 70: 167-180.

Zhang, Y., Koponen, S., Pulliainen, J. and Hallikainen, M. (1998), Landsat Thematic Mapper (TM) data analysis for chlorophyll-a and turbidity in the Gulf of Finland. *URSI/Remote Sensing Club of Finland/IEEE XXIII Convention on Radio Science and Remote Sensing Symposium*, pp. 69-70, 24-25August, Espoo, Finland.

Zhang, Y., Koponen, S., Pulliainen, J. and Hallikainen, M. (1999), Turbidity and Secchi disk depth analysis derived from Landsat Thematic Mapper data combined with ERS-2 data in the Gulf of Finland. *The 2nd Int. Symposium Operationalization of Remote Sensing*, August 16-20, ITC, Enschede, The Netherlands (CD ROM).

Zhang, Y., Koponen, S., Pulliainen, J. and Hallikainen, M. (2000), Turbidity detection using AVHRR satellite imagery in the Gulf of Finland. *URSI XXV Convention on Radio Science*, pp. 36-37, 21-22 September, Helsinki, Finland.

Zhang, Y., Pulliainen, J., Koponen, S., and Hallikainen, M. (2002a), Applicability of combined microwave and optical data for surface water quality retrievals. *Journal of Electromagnetic Waves and Applications*, 16: 249-251.

Zhang, Y., Pulliainen, J., Koponen, S., and Hallikainen, M. (2002b), Application of an empirical neural network to surface water quality estimation in the Gulf of Finland using combined optical data and microwave data. *Remote Sensing of Environment*, 81: 327-336.

Zhang, Y., Pulliainen, J., Koponen, S., and Hallikainen, M. (2002c), Water quality studies of combined optical, thermal infrared and microwave remote sensing. *Microwave and Optical Technology Letters*, 34: 281-285.

Zhang, Y., J. Pulliainen, S. Koponen, and M. Hallikainen, M. (2002d), Detection of Sea Surface Temperature (SST) using infrared band data of Advanced Very High Resolution Radiometer (AVHRR) in the Gulf of Finland. *International Journal of Infrared and Millimeter Waves*, 23: 1407-1412.

Zhang, Y., Pulliainen, J., Koponen, S., and Hallikainen, M. (2003a), Water quality retrievals from combined Landsat TM data and ERS-2 SAR data in the Gulf of Finland. *IEEE Trans. Geosci. Remote Sens.*, 41: 622-629.

Zhang, Y., Koponen, S., Pulliainen, J. and Hallikainen, M. (2003b), Application of empirical neural networks to chlorophyll-a estimation in coastal waters using optosensors. *IEEE Sensors Journal*, 3: 376-382.

Zhang, Y., Pulliainen, J., Koponen, S., and Hallikainen, M. (2003c), Empirical algorithms for Secchi disk depth using optical and microwave remote sensing data from the Gulf of Finland and the Archipelago Sea. *Boreal Environment Research*, 8: 251-261.